Buckling monopiles:

Stability of a monopile based offshore wind turbine

Thijs de Haan

Buckling monopiles:

Stability of a monopile based offshore wind turbine

by

Thijs de Haan

to obtain the degree of Master of Science
at the Delft University of Technology

Student number:	4314794	
Thesis committee:	Prof. dr. ir. A. Metrikine,	TU Delft, Chairman
	Ir. P. van der Male,	TU Delft, daily supervisor
	Ir. M. Versluis,	Witteveen+Bos, daily supervisor

An electronic version of this thesis is available at `http://repository.tudelft.nl/`.

TU Delft

Abstract

Offshore wind turbines are being placed all over the world. The increased popularity of these structures comes with a boost to the development of wind turbines in general, resulting in larger and higher constructions. To ensure the support structures of the turbines are able to withstand the extreme loads and environmental conditions, it is subjected to a series of tests and checks, prescribed by codes and standards. This thesis focuses on buckling checks, with global buckling in particular.

Several codes and standards define buckling checks, differing in approach. For example, the global buckling check is based on global buckling (compromised stability due to an axial force), but also takes eccentricities into account. How these parameters and safety factors are incorporated is analyzed for the Eurocode and the DNVGL, which are considered the most relevant design standards regarding offshore wind turbines around the Netherlands. Difference between both global buckling checks are analyzed using a monopile based reference wind turbine.

Looking to the more mechanical term of global buckling (also called Euler buckling), one finds an expression for the buckling load, based on the flexural stiffness and the buckling length of the structure. However, both parameters vary over the height of the support structure: the monopile has one relevant buckling value, where the flexural stiffness varies with its geometry. Therefore the buckling length cannot be constant for the structure. To tell something about this buckling length, the support structure is modeled with Euler beams as visualized in the figure. Subsequently the buckling force is analyzed, a constant value for the flexural stiffness is derived and the buckling length is calculated. Finally, the influence of the soil conditions on the buckling length of the structure is analyzed.

To determine whether a second order analysis is required to calculate the buckling force of the support structure, a comparison is made. Two Euler-Bernoulli beam models are introduced, one with a second order term, one without. The influence of the term on the bending, rotation, moment and shear force is analyzed, as well as the influence of the Euler buckling force. Subsequently an incremental load factor is introduced to incorporate the second order effect in the more simplified beam model.

Finally, the relevance of global buckling is considered. How relevant is the global buckling check for the currently installed wind turbines, and how relevant will it be for the larger support structures that are to be expected? To answer these questions, comparisons are made between the buckling checks and how far from failing the checks are. Subsequently, the local buckling is introduced to compare the global buckling check to the local buckling check regarding relevance.

Below, the most important results and conclusions are given below:

- The buckling check of the DNVGL and the Eurocode differ for result. However, the unity check is a factor 20 lower than critical.
- A buckling length of more than twice the length of the structure (from the seabed to the top) should be used for Euler buckling analysis.
- The second order term affects the total displacement- and moment distribution minimally: approximately 5% of the total moment (and displacement) is contributed by the second order term.
- Local buckling and global buckling are equally important, regarding the Eurocode. Both unity checks result in approximately the same values, which is a factor 20 away from being critical.

Preface

This thesis is written as final thesis for my MSc graduation for Offshore Engineering at the TU Delft. The reason for this thesis is the course where a support structure of an offshore wind turbine is to be designed and subjected to relevant standards. However, since the global buckling checks are defined rather vague, a master thesis is performed on the subject. My interest in the subject was found in the challange to perform a research in a rather unknown field for me. As most graduation projects, this one came with ups and downs, with a lot lessons learned.

During the graduation process I encountered several problems. My background knowledge was lacking and I struggled for months and months with the basics of the graduation subject. Subsequently the models were not working correctly. Another few months passed by with not much progress. When they finally worked I came up with a strategy to finalize the thesis. However, this is whe I found out that my daily supervisor was absent for a longer period, and would not help me finish my thesis. Without a daily supervisor I worked myself to this final thesis.

Finally, I want to thank everyone who has been involved in this project. Special thanks go to my daily supervisor Marco Versluis, who helped me at Witteveen+Bos. Thanks for the inspiring discussions we had about my thesis and kept me going in some dark times to my graduation. Pim van der Male, without you I would have followed a different road to graduation. During some lectures you inspired and fascinated me into offshore wind turbines. In our meetings we had countless discussion on the thesis, but also on other matters such as how to keep my motivation and how to prepare for the future. It was a shock when I discovered that Pim was absent for a long period, and could not help me finalize my thesis. I hope everything is better now.
I want to thank professor Andrei Metrikine for the time he has put in my thesis and the opportunity he gave me. He inspired me during the progress meetings to try and do better, no matter what.

Finally I want to thank everyone who was affected by my moods during my graduation. My housemates on the Brabo 70 had to deal with me when I was a bit down. Especially Thomas Aelen, who also helped me with the content of this thesis and came to Nijmegen for several weeks to write. My family inspired me to start my master, and kept inspiring me to finish it. Thanks for the kind words and tips on how to deal with some practical matters, they really opened my eyes. Thanks Gerrit-Jan, Jolien, Roel, Freek and Hannah!
Finally I want to thank my dearest Judith. She had to cope with me for over 2 years during my thesis, and supported me through this period mentally. I want to apologize for the evenings that I missed and the holidays that I skipped due to my thesis, and hope to make it up to you. The thing that inspired me the most during my graduation process was buying a house with you, renovating it and starting living together. I enjoyed it, moving to Nijmegen with you, and I am looking forward to enjoy it for some more...

Contents

1
Introduction

1.1. General introduction into offshore wind turbines

For over a century, wind has been used to produce electrical energy. Initially, the produced energy used to be stored in batteries, since access to a general power network was not yet established [SOURCE]. However, these days wind turbines are directly connected to general electrical power grid. Throughout the years the design of wind turbines showed growth in quantity, efficiency, power and reliability. The combination of these factors resulted in a reduced price per watt for a wind turbine, which makes the production, installation and operation of a wind turbine more cost effective and hence more attractive for investors. Figure 1.1 visualized the growth of both the average power and rotor diameter of a wind turbine throughout recent years. It is expected that this trend will continue: wind turbine manufacturer DONG Energy has announced their expectation that wind turbines in 2024 can produce 16 MW.[12].

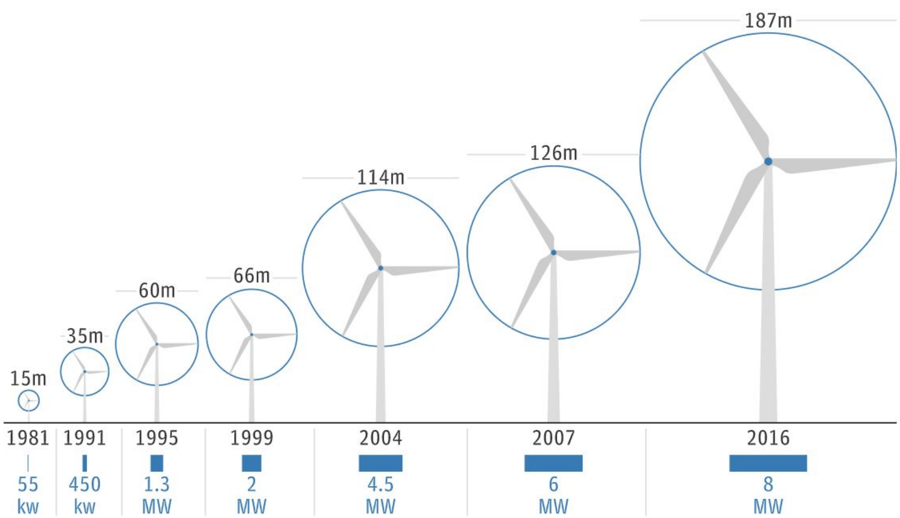

Figure 1.1: Power of a single wind turbines from 1985 - 2010 *(source: DONG Energy)*

Wind farms are situated at both on- and offshore locations. The advantage for offshore relates to the broad availability of suitable locations and the reliability of the wind compared to onshore locations. However, offshore wind farms do require an elaborate support structure to withstands weather and climate conditions that may occur at sea. The design of this support structure should consider the following conditions:

- Wind loads in operation and during storms;
- Sea-states including water elevation, waves and currents;
- Ice loading;
- Salt water: erosion of substructure and rotor-nacelle assembly (RNA);
- Scour;

- Marine growth.

1.2. Design of a support structure

The offshore wind industry relies on several types of support structures. The most common bottom founded support structures are as, visualized in Figure 1.2:

- Monopile;
- Tripod;
- Jacket;
- Gravity based.

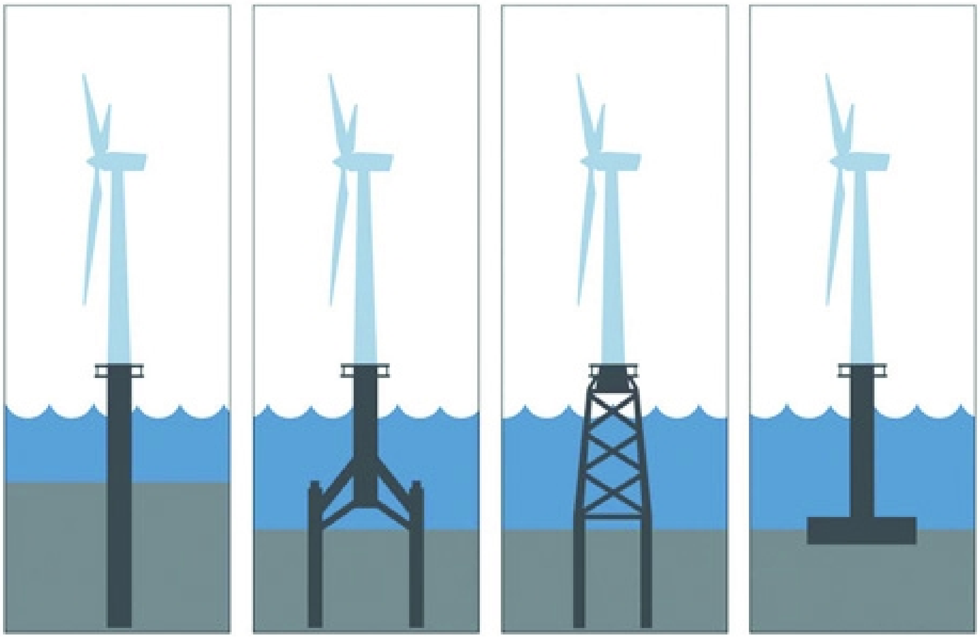

Figure 1.2: Support structure types (from left to right: monopile, tripod, jacket, gravity based)[12]

The most used substructure is the monopile. Due to its simplicity (a cold formed hollow tube with a large diameter), it is relatively easy to fabricate. With the specially developed monopile installation vessels, the installation process is being optimized, which reduces installation time and costs. Other types of substructures typically come with larger material-, fabrication- and/or installation costs.

A support structure is designed based on a couple of design criteria. One of these criteria is that it needs to withstand several combinations of loads. These load combinations are described in design standards as limit states. Several different limit states are distinguished[17]:

- Fatigue limit state (FLS);
- Serviceability limit state (SLS);
- Ultimate limit state (ULS).

These limit states define loads to assess the support structure for respectively its fatigue life, integrity during operation and resistance to extreme environmental conditions. For example, the fatigue of a support structure is assessed using the entire spectrum of expected environmental conditions over its serviceability life. However, the structural integrity is used using extreme environmental conditions, following from ULS load combinations. Checks performed with these ULS load combinations are enlisted below [4] [17]:

- Yield check: are the internal stress levels approaching the yield stress of the material;
- Global buckling check: is the structural stability due internal- and external loads being compromised;
- Local buckling check: is the stability locally being compromised, for example due to pressure differences.

- Foundation check: is the designed penetration depth in combination with the soil stiffness able to withstand extreme environmental conditions

Section 2 elaborates more on these checks. Both the Eurocode and DNVGL are discussed.

Figure 1.3 shows a typical layout of a monopile based wind turbine, including terminology. The subsoil- and submerged section is called the monopile. The section that is partially submerged, is called the transition piece. This section forms a connection between the monopile and the tower (top section). The transition piece often offers facilities such as a boat-landing or an external J-tube, to guide the power cable from the seabed to the tower, which is referred to as the top section of the support structure. The entire structure from subsoil to RNA is referred to as the support structure.

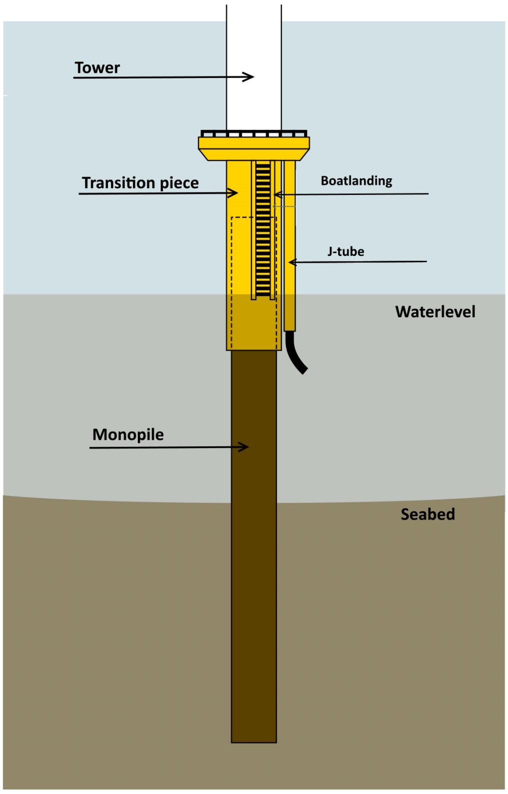

Figure 1.3: Terminology monopile based wind turbine

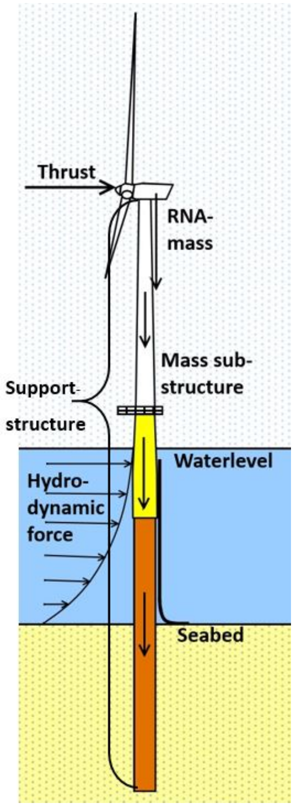

Figure 1.4: Loads on a monopile based offshore wind turbine

General loads exerted on the monopile are visualized in Figure 1.4. Horizontal loads are simplified as a locally applied thrust force and a distributed hydrodynamic force. Weight of both the support structure and the rotor nacelle assembly (RNA) is shown as vertical point loads, distributed over the height structure.

1.3. Problem statement

Buckling is a failure mode of a structure due to issues with stability. With regards to offshore monopiles, typically two types of buckling are distinguished: global buckling and local buckling. A visualization of both buckling types is shown in Figure 1.5. In this figure, global buckling occurs due to a vertical load only. When this vertical load reaches its buckling value, the structure may bend due to a small imperfection or load. Local buckling, however, is a failure mechanism that is occurs due to the stresses within the zone of an initial imperfections [1]. When the structure is perfect, without imperfections, local buckling will not occur. However, since every object is fabricated with tolerances and imperfections, local buckling will occur. Examples of imperfections are ovalisation in a round hollow tube, or surface damage.

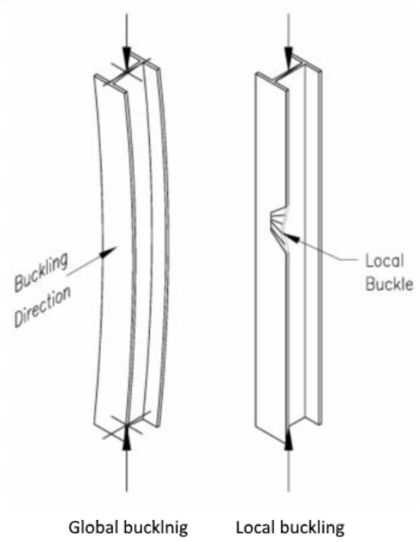

Figure 1.5: Global buckling (left) and local buckling (right) [13]

Global buckling is a failure that typically is initiated by a bend of a structure. This bend results in an internal moment, originating from the eccentricity of the mass of the structure. Due to this internal moment, a larger bend is obtained, which subsequently results in a larger eccentricity and a larger internal moment. This increasing internal moment is referred to as the second order moment[19].
The magnitude of the second order moment is affected by the length of the structure. When a longer structure bends, the eccentricity of its center of gravity is larger, resulting in a larger second order moment. However, the eccentricity of the center of gravity is affected by more parameters than the length of the structure only. Leonhard Euler defined an equations for so called Euler Buckling [19], applicable on the Euler-Bernoulli beam theory. Euler buckling takes boundary conditions of the structure into account, by considering an effective length, instead of the true length of the structure. Figure 1.6 visualizes several common situations, including its boundary conditions [19]. For example, the most left structure in this figure (denoted with a 1), is a cantilever beam with a rigid boundary condition in the bottom and a free boundary condition at the top.

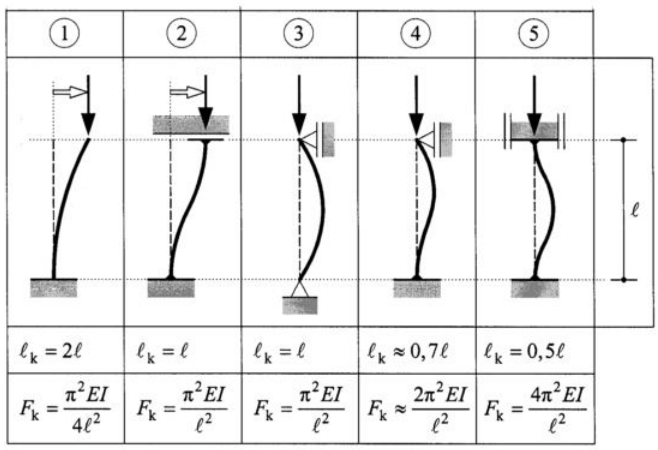

Figure 1.6: Several most common effective lengths [19]

Figure 1.7 plots the plastic yield strength (F_y) and the Euler strength of a beam, where the Euler strength is the resistance against Euler buckling and the slenderness parameter is based on the cross sectional geometry of the structure. Note that when one compares the Euler strength with the yield strength, a larger slenderness results in a lower buckling strength. However, when a bifurcation point between the plastic- and Euler strength is reached (as visualized in Figure 1.7), the yield strength of the material becomes dominant, and the column fails due to yielding. Around this bifurcation point, failure may occur at a lower load due to local effects. Also note that this figure is based on a structure without imperfections.

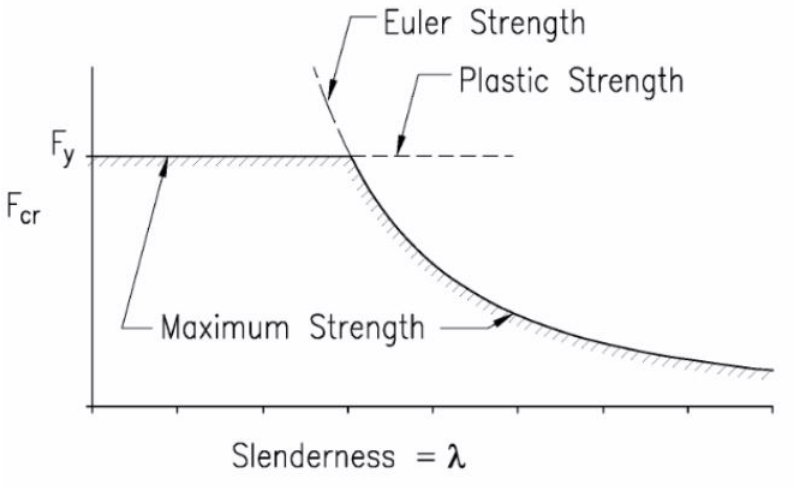

Figure 1.7: Plastic strength vs buckling strength [13]

The geometry of a support structure of an offshore wind turbine is a structure which should be checked for global buckling: the structure is a hollow tube with limited flexural stiffness and a mass on the top end. Due to horizontal loads, initiated by environmental conditions (wind and water forces), an eccentricity of the top mass is initiated. This eccentricity results in a second order moment in the support structure. A combination of the direction and magnitude of these parameters will initiate global buckling, which make it relevant for analysis.

Currently, designs of support structures for offshore wind turbines are subjected to a buckling check. These checks are defined by design standards, such as the Eurocode [4] and the DNVGL [3]. Several factors are taken into account, making the checks applicable for the support structure of an offshore wind turbine:

- Correction factor for the shape of the moment line;
- Reduction factor for used cross sectional geometry (due to the slenderness of the structure);
- Material factors;
- Reduction due to other imperfections.

These parameters are incorporated in a unity check. Section 2 elaborates on the buckling checks as per DNVGL and the Eurocode. However, since the support structure of an offshore wind turbine is embedded in soil, is built from sections with varying cross sectional properties, and is subjected to a variety of environmental conditions, a more complex system is obtained than, for example, visualized in Figure 1.6. This thesis elaborates on the encountered complexities, and how these are to be dealt with.

1.4. Research questions

Research questions are defined and used as guideline during this thesis. This allows a structured approach, resulting in clear results, discussion, conclusions and recommendations. All research questions are enlisted below. In section 1.5, the research questions are discussed, including the chosen approach. Note that research questions 1, 2, 3 and 4 refer to global buckling, and 4 includes analysis of local buckling.

1. Where do the differences regarding global buckling originate between the Eurocode and the DNVGL?
2. How should the buckling length of an offshore wind turbine be chosen?
3. Is a second order analysis required to determine whether global buckling is relevant in the design of an offshore wind turbine?
4. When does global buckling become relevant, referring to both extreme (design) conditions and local buckling?

1.5. Approach

1.5.1. Where do differences regarding global buckling originate between the Eurocode and the DNVGL?

A difference between the approach of the global buckling check of the Eurocode and DNVGL is noted. Both standards defined a unity check to assess wether global buckling is an issue or not. However, the structure of these unity checks differ by means of parameter definition. To obtain insight in the differences in the standards regarding the global buckling check, the standards are analyzed thoroughly by means of a base-case and an in-depth analysis of the used parameters. This research question is discussed in section 2.

1.5.2. How should the buckling length of an offshore wind turbine be chosen?

This research question follows from the standard Euler buckling cases. In these cases, as visualized in Figure 1.6, typical cases are defined for rigid-, free- and hinged boundary conditions. The length of the structure is factorized to an effective length, to include effects regarding buckling of the boundary conditions. However, since the support structure of a wind turbine is embedded in soil, one is dealing with a non-standard case. This research question is defined to determine how the effective length of a wind turbine like structure should be chosen. To do this, several cases are defined. Beginning with the derivation of the buckling force of a cantilever beam, the complexity of the support structure is increased, with for example a Winkler foundation for the subsoil section, and differences in cross sectional areas at the relevant elevations. The developments of the used models is discussed in section 3. The buckling length regarding the most complex model (including soil springs and diameter variations) is discussed in section 4.

1.5.3. Is a second order analysis required to determine whether global buckling is relevant in the design of an offshore wind turbine?

A model including a vertical force, variation in cross sections and an embedded section is defined to analyze the magnitude of the second order effect, with respect to a model without this second order term. The results regarding deflection and moment variations are compared, leading to a discussion regarding the relevance of this second order term in this application.
Furthermore, the final model is compared to the approach, as one follows regularly for the design of a monopile support structure (based on design standards). The results of both the model including the second order term and the approach per design standards are compared, analyzed and discussed in section 4 and 5.

1.5.4. When does global buckling become relevant?

The relevance of global buckling regarding an offshore wind turbine should be determined. A final model is defined which is used to determine the effect of different parameters. This model, consisting of varying cross sectional properties, a lateral thrust force, a distributed hydrodynamic force and a Winkler foundations for the sub-soil section, is derived in section 4. A more in depth analysis, including a parameter study is performed in section 5.
Also local buckling is included to determine when global buckling becomes relevant. A check based on design standards is performed using a reference wind turbine. Subsequently, variations in parameters are applied to verify when global buckling is relevant over local buckling.

2
Design standards

2.1. Introduction

For the design of a support structure of an offshore wind turbine, several checks are to be performed. Among others a global buckling check should be performed to ensure global buckling is will not occur. This buckling check is performed conform a design standard (such as the DNVGL and Eurocode). However, the buckling checks in these standards differ slightly.
This chapter elaborates on these global buckling checks, but also discusses a local buckling check. In a later chapter, these codes are compared and discussed regarding relevance. Research question 1, regarding the differences between the Eurocode and the DNV/GL is awnsered in section

2.2. DNVGL, global buckling check

The DNVGL is a collaboration between Det Norske Veritas and the Germanischer Lloyd. This standard describe among others what design criteria are for a support structure of an offshore wind turbine. This paragraph elaborates on the global buckling check that is to be carried out, to ensure global buckling will not occur. The check comes from following sources. [2][3][6]

The global buckling check is defined as a unity check:

$$\frac{N_d}{\kappa N_p} + \frac{\beta_m M_d}{M_p} + \Delta N \geq 1 \tag{2.1}$$

Where:

- N_d and M_d are respectively the design normal force and moment
- N_p and M_p are the resistance for resp. the normal force and moment
- κ is the flexural buckling coefficient
- β_m is the moment factor, determined with the moment line of the structure
- ΔN is the slenderness parameter.

For this buckling check the structure is modeled as a cantilever beam. The pile is fixed sub-soil (1 times the diameter beneath the soil) to account for the relative loose top layer of sand and scour. Now the plastic compression- and moment resistances are calculated:

$$N_p = \frac{A\sigma_y}{\gamma_M} \tag{2.2}$$

$$M_p = \frac{D\sigma_y}{2I\gamma_M} \tag{2.3}$$

$$M_p = \frac{W_p f_y}{\gamma_M} \tag{2.4}$$

$$W_p = \frac{D^3 - (D-2t)^3}{6} \tag{2.5}$$

Where:

- A is the cross sectional area
- D is the outer diameter of the pile
- t is the wall thickness of the pile
- W_p is the plastic section modulus
- σ_y is the yield stress of the material
- γ_M is the material factor

Now the reduced slenderness ratio λ and ϕ can be determined as follows:

$$\lambda = \sqrt{\frac{N_p \gamma_M}{N_{ki,d}}} \tag{2.6}$$

$$\phi = 0.5(1 + \alpha(\lambda - 0.2) + \lambda^2) \tag{2.7}$$

Where α is valued 0.2 and $N_{ki,d}$ is the (normal) elastic buckling force, calculated below.

$$N_{ki,d} = \frac{\pi^2 EI}{L_{buck}^2} \tag{2.8}$$

Where E is the elasticity modulus of the steel and L_{buck} is the length of the pile from soil to top, enlarged with 1 time the diameter of the pile to take the loose top soil layer into account.
With above parameters determined, the flexural buckling κ can be determined:

$$\kappa = \begin{cases} 1.0, & \text{for} \quad \lambda \leq 0.2 \\ \frac{1}{\phi + \sqrt{\phi^2 - \lambda^2}}, & \text{for} \quad \lambda \geq 0.2 \end{cases} \tag{2.9}$$

N_d and M_d follow from the loads on the monopile. The normal design force is a combination of the masses of the pile and rotor nacelle assembly (RNA), where the value for the design moment is determined by the thrust force and the wave loading.

Finally, the slenderness parameter Δn can be determined, which is an additional safety factor depending on the slenderness of the system.

$$\Delta n = min(0.25\kappa\lambda^2, 0.1) \tag{2.10}$$

With all discussed parameters the unity check can be entered and the global buckling check can be performed. Reference is made to section 5.5 where the DNVGL and the Eurocode are compared.

2.3. Eurocode, global buckling check

For a cross section, 4 classes are defined. These cross sectional classes define what the leading design parameters should be regarding several checks (among others the yield stress check and the buckling checks). We are interested in the class regarding a monopile based offshore wind turbine. This type of structure is classified as class 3:

'Class 3 cross-sections are those in which the stress in the extreme compression fiber of the steel member assuming an elastic distribution of stresses can reach the yield strength, but local buckling is a liable to prevent development of the plastic moment resistance.'

The buckling check in the Eurocode is comparable to those in the DNV and GL. The unity check that is to be assessed is given below:

$$\frac{N_{Ed}}{\frac{\chi_y N_{Rk}}{\gamma_{M1}}} + k_{zy}\frac{M_{y,Ed} + \Delta M_{y,Ed}}{\frac{\chi_{LT} M_{y,Rk}}{\gamma_{M1}}} + k_{zz}\frac{M_{z,Ed} + \Delta M_{z,Ed}}{\frac{M_{z,Rk}}{\gamma_{M1}}} \leq 1 \tag{2.11}$$

$$\frac{N_{Ed}}{\frac{\chi_z N_{Rk}}{\gamma_{M1}}} + k_{yy}\frac{M_{y,Ed}+\Delta M_{y,Ed}}{\frac{\chi_{LT} M_{y,Rk}}{\gamma_{M1}}} + k_{yz}\frac{M_{z,Ed}+\Delta M_{z,Ed}}{\frac{M_{z,Rk}}{\gamma_{M1}}} \leq 1 \tag{2.12}$$

Where:

- N_{Ed},$M_{y,Ed}$ and $M_{z,Ed}$ are resp. the design normal force and bending moment in resp. the y- and z-directional bending
- $\Delta M_{y,Ed}$ and $\Delta M_{z,Ed}$ are the moment due to the shift of the centroidal axis due to bending
- χ_z,χ_y and χ_{LT} are resp. the flexural buckling term and the the reduction factor due to lateral torsional buckling
- k_{yy} and k_{yz} and k_{zy} are interaction factors
- γ_{M1} is a partial factor for resistance of members to instability assessed by member check

We look more in detail to these parameters in the table below.

Table 2.1: Eurocode global buckling parameters

Parameter	**Unit**	**Description**
N_{Ed}	N	Calculated as summation of the RNA mass and tower weight
$M_{i,Ed}$	Nm	Moment in the structure as result of lateral forces
$\Delta M_{i,Ed}$	Nm	For class 4 cross sections, this parameter may be neglected.
χ_z	–	Is determined using so-called buckling curves.
χ_{LT}	–	This lateral torsionnal component is 1, since torsion is not taken within the scope of this check
N_{Rk}	N	This resistance parameter is defined as $N_{Rk} = f_y A$
$M_{i,Rk}$	Nm	This resistance parameter is defined as $M_{i,Rk} = f_y W_{el,i}$
k_{ii}	–	These interaction factors are calculated below.

Note that the torsion is not taken into account, hence, after simplifying with the assumptions as per Table 2.1, the following unity check remains:

$$\frac{N_{Ed}}{\frac{\chi_z N_{Rk}}{\gamma_{M1}}} + k_{yy}\frac{M_{y,Ed}}{\frac{\chi_{LT} M_{y,Rk}}{\gamma_{M1}}} \leq 1 \tag{2.13}$$

χ_z is determined. From the code we obtain the buckling curves in Figure 2.1. Since a monopile is a hollow circular shaped cross section we use curve c. Now the non-dimensional slenderness parameter $\overline{\lambda}$ is calculated.

$$\overline{\lambda} = \sqrt{\frac{Af_y}{N_{cr}}} \tag{2.14}$$

Where:

- A is the cross sectional area of the monopile. For the reference model, a value of 1.1 $[m^2]$ is used.
- f_y denotes the yield stress of the material, typically around $250MPa$.
- N_{cr} is the Euler Buckling force

$$N_{cr} = \frac{\pi^2 EI}{(2L)^2} \tag{2.15}$$

From Figure 2.1, we can find a value for χ_z.

Finally the coupling term k_{yy} is being determined. This term is dependent on the type of structure (type 3), as given below:

$$k_{yy} = C_{my} C_{mLT} \frac{\mu_y}{1-\frac{N_{Ed}}{N_{cr}}} \tag{2.16}$$

$$C_{my} = 1 = 1 + \left(\frac{\pi^2 EI|\delta_x|}{L^2|M_{Ed}(x)}| - 1\right)\frac{N_{Ed}}{N_{cr}} \tag{2.17}$$

$$C_{mLT} = 1,0 \tag{2.18}$$

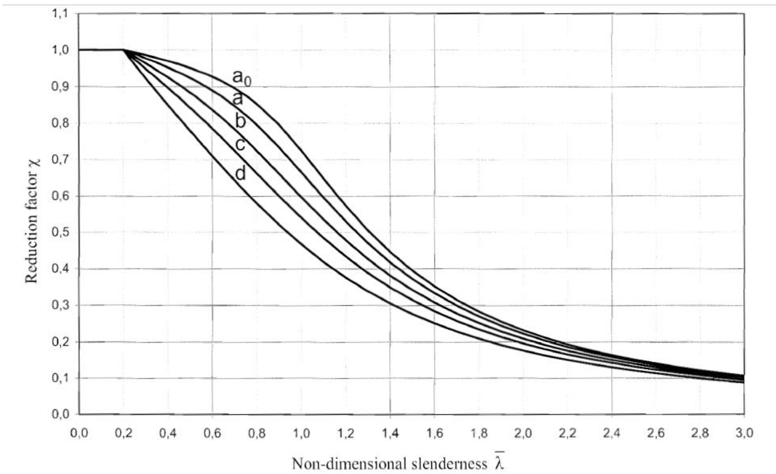

Figure 2.1: Buckling curves, curve c for hollow circular cross sections

$$\mu_y = \frac{1 - \frac{N_{Ed}}{N_{cr}}}{1 - \chi_y \frac{N_{Ed}}{N_{cr}}} \tag{2.19}$$

With this, all parameters regarding the global buckling check as per Eurocode are discussed. Section 5.5 elaborates on this check by applying it to the reference wind turbine.

2.4. Eurocode, local buckling check

To determine when global buckling becomes relevant with regards local buckling, a local buckling check is defined. The Eurocode discusses two types of local buckling check: stress- and strain based checks.
The stress based local buckling check used in this thesis is discussed in the Eurocode-1993-6 [5] and summarized below. Figure 2.2 shows an overview of the symbol and sign definition regarding this local buckling check.

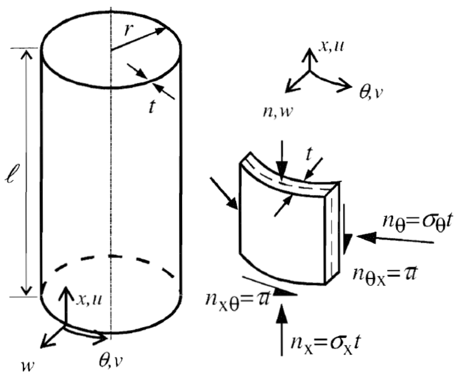

Figure 2.2: Symbol and sign definition local buckling of a cylindrical shell

$$\left(\frac{\sigma_{x,Ed}}{\sigma_{x,Rd}}\right)^{k_x} + k_i \left(\frac{\sigma_{x,Ed}}{\sigma_{x,Rd}}\right)\left(\frac{\sigma_{\theta,Ed}}{\sigma_{\theta,Rd}}\right) + \left(\frac{\sigma_{\theta,Ed}}{\sigma_{\theta,Rd}}\right)^{k_\theta} + \left(\frac{\tau_{x\theta,Ed}}{\tau_{x\theta,Rd}}\right)^{k_\tau} \leq 1 \tag{2.20}$$

With:

- σ_x is the meridional buckling stress
- σ_θ is the circumferential buckling stress
- $\tau_{x\theta}$is the buckling shear stress

- $k_x, k_\theta, k_\tau, k_i$ buckling interaction parameter

Since the pile is hollow and filled with sea water (up to sea level), the inside pressure is equal to the outside pressure. Therefore there is no significant circumferential stress. The terms relevant to circumferential buckling are therefore small, and may be neglected, resulting in the following unity check (dependent on the compressive stress and lateral shear components):

$$\left(\frac{\sigma_{x,Ed}}{\sigma_{x,Rd}}\right)^{k_x} + \left(\frac{\tau_{x\theta,Ed}}{\tau_{x\theta,Rd}}\right)^{k_\tau} \leq 1 \tag{2.21}$$

The resistance- and design parameters regarding the compression- and shear stresses on the pile are discussed more thoroughly in section XX. Below, relevant buckling interaction parameters are discussed.

The length of the shell segment is characterised by ω, which subsequently is used to determine the critical meridional buckling stress $\sigma_{x,Rcr}$.

$$\omega = \frac{l}{\sqrt{rt}} \tag{2.22}$$

$$\sigma_{x,Rcr} = 0.605EC_x\left(\frac{r}{t}\right) \tag{2.23}$$

With:

- r is the radius of the pile;
- t is the thickness of the pile;
- C_x depends on ω, for this thesis taken as $1,0$ (medium long cylinder).

$$k_x = 1.25 + 0.75\chi_x \tag{2.24}$$

Where χ_τ depends on the relative slenderness $\overline{\lambda}_x$.

$$\overline{\lambda}_x = \sqrt{f_{yk}/\sigma_{x,Rcr}} \tag{2.25}$$

$$\sigma_{x,Rcr} = 0,60EC_x\frac{t}{r} \tag{2.26}$$

$$\overline{\lambda}_{px} = \sqrt{\frac{\alpha}{1-\beta}} \tag{2.27}$$

$$\alpha_x = \frac{0,62}{1+1,91(\Delta w_k/t)^{1,44}} \tag{2.28}$$

$$\Delta w_k = \frac{1}{Q}\sqrt{\frac{r}{t}}t \tag{2.29}$$

with:

- the meridional squash limit slenderness $\overline{\lambda}_{x0}$ is taken as $0,20$
- Q is teh compression fabrication quality parameter, taken as 25 (high).
- Plastic range factor β is 0,60.
- f_{yk} is the characteristic yield strength ($335N/mm^2$)

Subsequently the buckling interaction parameter k_τ is calculated:

$$k_\tau = 1.75 + 0.25\chi_\tau \tag{2.30}$$

$$\overline{\lambda}_\tau = \sqrt{\left(f_{yk}/\sqrt{3}\right)/\tau_{x\theta,Rcr}} \tag{2.31}$$

$$\overline{\lambda}_{p\tau} = \sqrt{\frac{\alpha}{1-\beta}} = \sqrt{\frac{0,60}{1-0,65}} = 1,3093 \tag{2.32}$$

$$\tau_{x\theta,Rcr} = 0,75EC_\tau\sqrt{\frac{1}{\omega}}\frac{t}{r} \tag{2.33}$$

Where C_τ is 1,0 (medium length cylinder) and $\lambda_{\tau 0}$ is equal to $0,40$. For the base case as discussed in section 4 the following applies: $\lambda_{tau} \leq \lambda_{\tau 0}$, $\chi_\tau = 1,0$.

Finally, all parameters are discussed to determine the design- and resistance stresses for the unity check. $\sigma_{x,Rd}$ and $\tau_{x\theta,Rd}$ are determined:

$$\sigma_{x,Rd} = \frac{\chi_x f_{yk}}{\gamma_{m1}} \tag{2.34}$$

$$\tau_{x\theta,Rd} = \frac{\chi_\tau f_{yk}}{\sqrt{3}\gamma_{m1}} \tag{2.35}$$

With safety factor $\gamma_{m1} = 1,1$.

2.5. Differences global buckling check Eurocode-DNVGL

Comparing both checks, many equalities are found, as listed below:

- Both the Eurocode and the DNVGL define the check as a unity check
- Both the normal force and moments are taken into account;
- The maximum allowed normal force is factorized by a global buckling factor, taking the slenderness and sensitivity to global (Euler) buckling into account;
- Another parameter is introduced to factorize the resistance of a bending moment to account for the slenderness.
- Both checks take several safety factors into account, to allow for small (fabrication) errors.

However, more interestingly is where differences occur. These are found in the safety factors. Where the Eurocode elaborates on these safety factors in more detail than the DNVGL, a higher accuracy is obtained. Subsequently, the DNVGL takes a larger safety factor into account, likely resulting in a more conservative result.

3

Theoretical framework

3.1. Introduction

In this chapter a model is developed that is used to obtain insight in buckling of a support structure of an offshore wind turbine, leading to a final model. The final model is used to answer research questions 3 and 4, and is discussed in chapter 4. However, to validate and understand the final model, a range of intermediate models is obtained. These models will offer insight in the relevance of different components of the final model. Also, this chapter will lead to the answer of research question 2. This means that Euler buckling is evaluated, including a reduction factor regarding effective length, that serve as modules for the final model.

Starting at a uniform cantilever beam with only a vertical load, more parameters are added. An overview of the discussed models is given below. The models are derived and discussed more thoroughly in the paragraphs to come. A visualization of the models is given in Figure 3.1, and will be discussed separately in the following paragraphs. Firstly, a definition of the model is given, including general assumptions.

1. Cantilever beam with axial load (Figure 3.1 a);
2. Free-free beam with axial load and soil springs (Figure 3.1 b);
3. Free-free beam with axial load and partly embedded in soil springs (Figure 3.1 c);
4. Cantilever beam with axial load and lateral load (Figure 3.1 d);
5. Free-free beam with axial load, lateral load and soil springs (Figure 3.1 e).

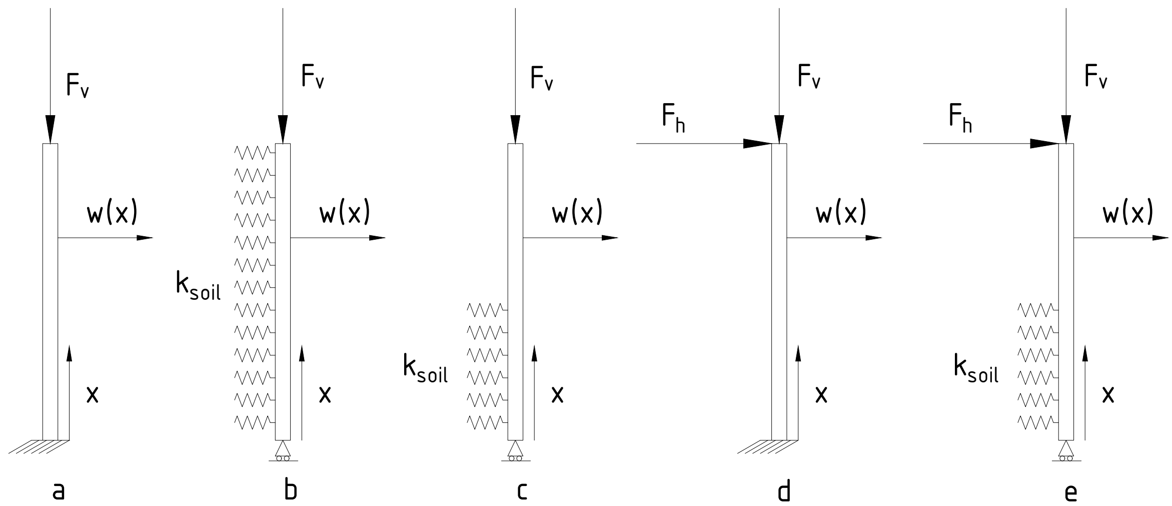

Figure 3.1: Different beam models

3.2. Beam theory

An offshore monopile is typically modeled as a bending beam, using on of many beam theories. The Timoshenko beam theory and the Euler-Bernoulli beam theory [14] are mostly used for structures such as the monopile of an offshore wind turbine. However, for offshore monopile-like structures, no significant differences in results is noted [10].
Higher order and more sophisticated beam theories such as Ghughal [16] and Reddy [7] are considered. However, it is noted that these higher order beam theories make the model unnecessary complicated [10]. Therefore one can conclude that results obtained with the simpler beam theory such as the Euler and Timoshenko beam theories, suffice for the model as defined in this thesis.
Since the researcher is more familiar with the Euler Bernoulli beam theory, this theory is used throughout this thesis.

3.3. Model definition

3.3.1. General assumptions

A semi-analytical model is developed. Several assumptions are made, which are discussed in this paragraph. The analytical model is developed using the Euler-Bernoulli beam theory (reference is made to section 3.2. A general form of the ordinary differential equation, containing all relevant parameters, is given below. Subsequently, each parameter is discussed regarding assumption and simplifications. Note that $w(x)$ denotes the deflection of the beam at elevation x.

$$EI(x)\frac{d^4w(x)}{dx^4} + F_v(x)\frac{d^2w(x)}{dx^2} + k_{soil}(x)w(x) = q(x) \tag{3.1}$$

- $EI(x)$ is the flexural stiffness of the beam. This parameter consists of the elasticity modulus (E), and the moment of inertia (I). Since the moment of inertia is dependent on among other the diameter and wall thickness of the pile, a variation per elevation is noted. However, it is assumed that the cross sectional parameters of each section remains constant, and therefore: $EI(x) = EI$. Note that the flexural stiffness may vary between the used sections.
- $F_v(x)$ is the vertical force component in the pile, initiated by gravity (including the top mass and the mass of the pile). Since the mass of a pile is distributed over the length of the pile, F_v varies over the height x. However, to simplify the models and due to insignificance of the weight of the pile with respect to the top mass, it is assumed that F_v is constant over a single section of the beam. Thus: $F_v(x) = F_v$.
- $k_{soil}(x)$ denotes a stiffness of a soil. This parameter typically varies over the depth of the soil. However, it is assumed that this parameter is constant over the sub-soil section to simplify the analysis. Therefore: $k_{soil}(x) = k_{soil}$. Reference is made to section4.4.2 for more details on the soil stiffness parameter.
- $q(x)$ denotes a distributed horizontal load. This parameter is used to define a hydrodynamic force over the submerged section of the support structure. Details on this parameter are discussed in section 3.8.

Rewriting and incorporating above assumptions gives a more workable form:

$$\frac{d^4w(x)}{dx^4} + \alpha^2\frac{d^2w(x)}{dx^2} + \beta w(x) = \frac{q(x)}{EI} \tag{3.2}$$

Where $\alpha^2 = \frac{F_v}{EI}$ and $\beta = \frac{k_{soil}}{EI}$

Relation between the deflection $w(x)$, rotation $\phi(x)$, moment $M(x)$ and shear force $V(x)$ are given below. The directions of the signs are defined in Figure 3.2.

$$\phi(x) = -\frac{dw(x)}{dx} \tag{3.3}$$

$$M(x) = -EI\frac{d^2w(x)}{dx^2} = EI\frac{d\phi(x)}{dx} \tag{3.4}$$

$$V(x) = -EI\frac{d^3w(x)}{dx^3} = EI\frac{d^2\phi(x)}{dx^2} = EI\frac{dM(x)}{dx} \tag{3.5}$$

Since one is interested in the horizontal force component (due to the horizontal thrust- and hydrodynamic force), and not in the perpendicular forces, a horizontal force component S_z is defined.

$$S_z(x) = V(x) + F_v\phi(x) \tag{3.6}$$

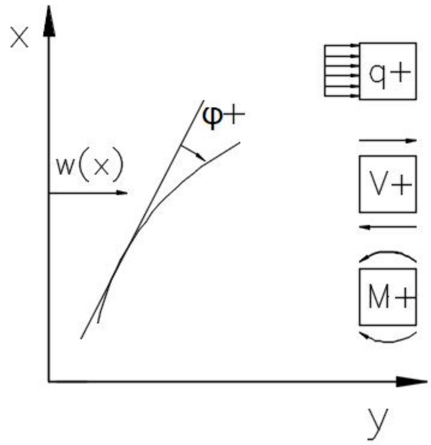

Figure 3.2: Definition signs

3.3.2. Reference offshore wind turbine

A reference turbine is defined to use as guideline regarding parameter definition throughout this thesis. This reference turbine, including support structure and environmental conditions, is based on 2 reports: *Definition of a 5-MW Reference Wind Turbine for Offshore System Development* [8] discusses the "NREL offshore 5-MW baseline wind turbine" in detail. Several support structures with relevant environmental conditions are discussed in *Support Structure Concepts for Deep Water Sites* [18] by UpWind.

Throughout this chapter reference is made to these reports, containing relevant design parameters. Note that due to simplifications regarding geometry and load, a set op simplified parameters is defined. These parameters are discussed more in depth in chapter 4.

3.4. Cantilever beam with vertical load

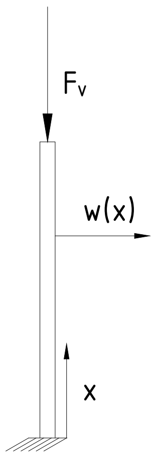

Figure 3.3: Beam model with vertical force

The equation of motion of this beam is based on equation 3.2, as given below:

$$\frac{d^4 w(x)}{dx^4} + \alpha^2 \frac{d^2 w(x)}{dx^2} + \beta(x) w(x) = \frac{q(x)}{EI} \tag{3.7}$$

However, since this cantilever beam is free of soil ($k_{soil} = 0$) and does not contain a distributed load ($q(x) = 0$, the equation is simplified to:

$$\frac{d^4 w(x)}{dx^4} + \alpha^2 \frac{d^2 w(x)}{dx^2} = 0 \tag{3.8}$$

With $\alpha^2 = F_v/EI$
Boundary conditions at the top and the bottom of the beam are defined as resp. free and clamped, mathematically represented by the following relations:

$$x = 0: \quad w = 0 \quad \text{and} \quad \phi = 0$$
$$x = L: \quad M = 0 \quad \text{and} \quad S_z = 0$$

A definition of $w(x)$ is required to obtain a workable solution. The following form is tried:

$$w(x) = \sum_{n=1}^{4} C_n e^{i\lambda_n x} \tag{3.9}$$

Where λ_n denotes the eigenvalues of the system and C_n are integration constants. We obtain λ from the characteristic equation, given below.

$$\lambda^4 + \alpha^2\lambda^2 = \lambda^2(\lambda^2 - \alpha^2) = 0 \tag{3.10}$$

$$\lambda_{1,2} = \pm(\alpha) \qquad\qquad \lambda_{3,4} = 0 \tag{3.11}$$

Solving this standard ordinary differential equation problem, we obtain the following equation for $w(x)$. Note that subsequently this equation is written in a more convenient form, where C_1 and C_2 are not equal to $\tilde{C}_1$ and $\tilde{C}_1$

$$w(x) = C_1 e^{i\alpha x} + C_2 e^{-i\alpha x} + C_3 x + C_4 = \tilde{C}_1 cos(\alpha x) + \tilde{C}_2 sin(\alpha x) + C_3 x + C_4 \tag{3.12}$$

This solution is derived to the following relations:

$$\phi(x) = \tilde{C}_1 \alpha sin(\alpha x) - \tilde{C}_2 \alpha cos(\alpha x) - C_3 \tag{3.13}$$

$$M(x) = \tilde{C}_1 F_v cos(\alpha x) + \tilde{C}_2 F_v sin(\alpha x) \tag{3.14}$$

$$V(x) = -\tilde{C}_1 F_v \alpha sin(\alpha x) + \tilde{C}_2 F_v \alpha cos(\alpha x) \tag{3.15}$$

$$S_z(x) = V(x) + F_v\phi(x) = -\tilde{C}_1 F_v \alpha sin(\alpha x) + \tilde{C}_2 F_v \alpha cos(\alpha x) + F_v(\tilde{C}_1 \alpha sin(\alpha x) - \tilde{C}_2 \alpha cos(\alpha x) - C_3) \tag{3.16}$$

$$S_z(x) = F_v C_3 \tag{3.17}$$

Substituting these relations in the boundary conditions, one obtains a system of equation, as given in the matrix equations below:

$$\begin{bmatrix} 1 & 0 & 0 & 1 \\ 0 & -\alpha & -1 & 0 \\ EI\alpha^2 cos(\alpha L) & +EI\alpha^2 sin(\alpha L) & 0 & 0 \\ 0 & 0 & -F_v & 0 \end{bmatrix} \begin{bmatrix} \tilde{C}_1 \\ \tilde{C}_2 \\ C_3 \\ C_4 \end{bmatrix} = 0 \tag{3.18}$$

Since one is not interested in the trivial solution, it can be concluded that the constants C_3 and $\tilde{C}_2$ are 0. We obtain the following system:

$$\begin{bmatrix} 1 & 1 \\ EI\alpha^2 cos(\alpha L) & 0 \end{bmatrix} \begin{bmatrix} \tilde{C}_1 \\ C_4 \end{bmatrix} = 0 \tag{3.19}$$

When the determinant of the given matrix is equal to 0, a solution is found.

$$det \begin{bmatrix} 1 & 1 \\ EI\alpha^2 cos(\alpha L) & 0 \end{bmatrix} = -EI\alpha^2 cos(\alpha L) = 0 \tag{3.20}$$

This is the case when $cos(\alpha L) = 0$, thus $\alpha L = \frac{1}{2}n\pi$, where n gives the mode of the system ($n = 1, 2, , ...n$). The lowest value where buckling occurs is for n=1, corresponding to the lowest buckling mode of this structure. A higher value for n denotes a higher order buckling mode.
$\alpha = \sqrt{F_v/EI} = \frac{\pi}{2L}$

$$F_{buck} = \frac{EI\pi^2}{4L^2} \tag{3.21}$$

Table 3.1: Design parameters partly embedded beam

Parameter		Unit	Description
E	210	$[GPa]$	Elasticity modulus
D_{pile}	6	$[m]$	Pile diameter
t_{pile}	0.06	$[m]$	Wall thickness
L	104	$[m]$	Length of pile (from seabed to RNA)

When looking back to Figure 1.6, it can be concluded that the obtained solution is equal to the rule of thumb, as given in standard case 1 (cantilever beam).
To check with what order of buckling forces one is dealing, a set of parameters is defined to analyze the buckling force of a cantilever beam. Table 3.1 gives the magnitude of the relevant parameters. Note that the values are fictional, but based on the reference model.

$$F_{buck} = \frac{EI\pi^2}{4L^2} = 236MN \tag{3.22}$$

3.5. Free-free beam with soil springs

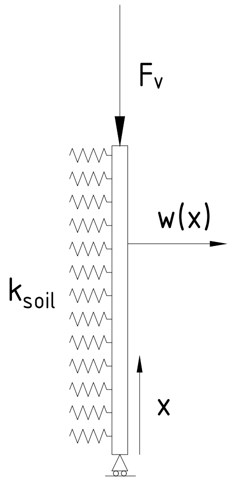

Figure 3.4: Beam model with vertical force and soil springs

The governing equations are as equation 3.2. In this case, the distributed force $q(x)$ is equal to 0, and thus the following equation is obtained:

$$\frac{d^4w(x)}{dx^4} + \alpha^2\frac{d^2w(x)}{dx^2} + \beta w(x) = 0 \tag{3.23}$$

With: $\alpha^2 = \frac{F_v}{EI}$ and $\beta = \frac{k_{soil}}{EI}$
We are looking for a solution in the following form:

$$w(x) = \sum_{n=1}^{4} C_n e^{i\lambda_n x} \tag{3.24}$$

The characteristic equation is defined, and solved for the eigenvalue, where λ denotes this eigenvalue of the system.

$$\lambda^4 + \alpha^2\lambda^2 + \beta = 0 \tag{3.25}$$

$$\lambda^2 = -\frac{\alpha^2}{2} \pm \sqrt{\left(\frac{\alpha^2}{2}\right)^2 - \beta} \tag{3.26}$$

Given that both the soil stiffness k_{soil} and compressive force F_v are positive, two cases are distinguished, based on the real and complex roots of the eigenvalues:

1. Case 1: $\alpha^4/4 < \beta$: Roots contain a real- and an imaginary part.
2. Case 2: $\alpha^4/4 > \beta$: All roots are completely imaginary.

A quick calculation offers insight in which region the reference offshore wind turbine is found. Magnitudes of the used values are based on the reference wind turbine. Note that these values are meant to obtain insight what case is expected to be relevant for this study.

$$\alpha = \frac{F_v}{EI} = \frac{350e3 \times 9.81[N]}{10^{12}[Nm^2]} = 10^{-6}[m^{-2}] \qquad \beta = \frac{k}{EI} = \frac{10^8[N/m^2]}{10^{12}[Nm^2]} = 10^{-4}[m^{-2}] \tag{3.27}$$

$$\frac{\alpha^4}{4} - \beta = \frac{(10^{-6})^4}{4} - 10^{-4} << 0 \tag{3.28}$$

Thus case 1 is relevant for this case. When the vertical force F_v is increased to the magnitude of buckling value ($F_v = 1e9$, $\alpha = 1e-3$), which is relevant for buckling analysis, the comparison will result as follows, concluding that by a significant difference in magnitude in values for the relevant parameters, one is still dealing with case 1.

$$\frac{\alpha^4}{4} - \beta = \frac{(10^{-3})^4}{4} - 10^{-4} << 0 \tag{3.29}$$

Below, both case 1 and case 2 are discussed more thoroughly.

Case 1: $(\alpha^4/4) < \beta$
The eigenvalues for the beam with Winkler foundations are given and rewritten:

$$\lambda^2 = -\frac{\alpha^2}{2} \pm \sqrt{\left(\frac{\alpha^2}{2}\right)^2 - \beta} \tag{3.30}$$

$$\lambda^2 = -\left(\frac{\alpha}{2} + i\sqrt{\beta - \left(\frac{\alpha}{2}\right)^2}\right) \quad , \quad -\left(\frac{\alpha}{2} - i\sqrt{\beta - \left(\frac{\alpha}{2}\right)^2}\right) \tag{3.31}$$

Using algebra, the eigenvalues are rewritten to a more convenient form:

$$\lambda = \pm P \pm iQ \tag{3.32}$$

With:

$$P = \sqrt{\sqrt{\frac{\beta}{4}} + \frac{\alpha}{4}} \qquad Q = \sqrt{\sqrt{\frac{\beta}{4}} - \frac{\alpha}{4}} \tag{3.33}$$

Substituting these eigenvalues in the general solution as in equation 3.24, one obtains the following:

$$w(x) = C_1 e^{(P+Qi)x} + C_2 e^{(P-Qi)x} + C_3 e^{(-P+Qi)x} + C_4 e^{(-P-Qi)x} \tag{3.34}$$

Using Eulers formula $e^{ix} = \cos(x) + i\sin(x)$, we can rewrite the general solution to trigonometric form. Note that $C_n \neq \tilde{C_n}$

$$w(x) = \tilde{C}_1 e^{Px}\cos(Qx) + \tilde{C}_2 e^{Px}\sin(Qx) + \tilde{C}_3 e^{-Px}\cos(Qx) + \tilde{C}_4 e^{-Px}\sin(Qx) \tag{3.35}$$

Note that this general solution is used for all following models, where soil springs are used.

Case 2: $(\alpha/2)^2 \geq \beta$
However, the solution of case 2 is less relevant for the analysis of buckling, the general solution is derived below.

When $(\alpha/2)^2 \geq \beta$, pure imaginary eigenvalues are obtained. The eigenvalues will become:

$$\lambda^2 = -\left(\frac{\alpha}{2} + \sqrt{\beta - \left(\frac{\alpha}{2}\right)^2}\right) \quad , \quad -\left(\frac{\alpha}{2} - \sqrt{\beta - \left(\frac{\alpha}{2}\right)^2}\right) \tag{3.36}$$

$$\lambda_{1,2} = \pm i\sqrt{\frac{\alpha}{2} + \sqrt{\left(\frac{\alpha}{2}\right)^2 - \beta}} \quad , \quad \lambda_{3,4} = \pm i\sqrt{\frac{\alpha}{2} - \sqrt{\left(\frac{\alpha}{2}\right)^2 - \beta}} \tag{3.37}$$

Substituting these eigenvalues in equation 3.24 and subsequently converting to a trigonometric function, concludes the following function:

$$w(x) = \tilde{C}_1 \cos(\lambda_1 x) + \tilde{C}_2 \sin(\lambda_1 x) + \tilde{C}_3 \cos(\lambda_3 x) + \tilde{C}_4 \sin(\lambda_3 x) \tag{3.38}$$

Note that this case is not relevant regarding any buckling study. Case 1 contains lower values for the vertical force, including several buckling forces.

3.5.1. Buckling force

The general solution is determined (equation 3.35). To obtain a set of equations, describing the subsoil beam, boundary conditions are defined:

$$\begin{aligned} x = 0: &\quad M = 0 \quad \text{and} \quad S_z = 0 \\ x = L: &\quad M = 0 \quad \text{and} \quad S_z = 0 \end{aligned}$$

The moment M and horizontal force S_z are derived as per equations 3.3 to 3.6. Combining these relations with the boundary conditions gives a set of governing equations. For the sake of convenience (the obtained solutions are long), these relations are determined in using mathematical software Maple, and not given here.

The obtained set of equations can be written in matrix form. Table 3.2 gives magnitudes of the used parameters. Note that the given values are fictional, but based on the reference wind turbine.

Table 3.2: Design parameters subsoil

Parameter		Unit	Description
E	210	$[GPa]$	Elasticity modulus
k_{soil}	$1e8$	$[N/m^2]$	Soil stiffness
D_{pile}	6	$[m]$	Pile diameter
t_{pile}	0.06	$[m]$	Wall thickness
L	28	$[m]$	Penetration depth of the pile

The determinant of the set of governing equations is determined and equalized to 0 ($det(M_{subsoil} = 0)$). When this equation is satisfied, the stability of the beam is compromised and buckling will occur. Figure 3.5 plots the logarithmic value of the determinant to the vertical force F_v. Note that the first buckling force is reached around $F_v = 6e9N$. However, when a larger penetration depth is chosen, a larger buckling force is obtained (reference is made to Figure 3.6, which shows the stabilizing properties of soil springs.

When comparing these buckling forces to that of a cantilever beam (as obtained in section 3.4), a significant difference is noted: $F_{buck,cantilever} = \frac{EI\pi^2}{4L^2} = 2.5e8$), which is a factor 40 lower than the buckling force of the embedded beam. This significant difference is caused by the stabilizing effect of the soil springs. When the beam bends, a force in the opposite direction acts on the beam. This force works counter-bending, and with that counter-buckling.

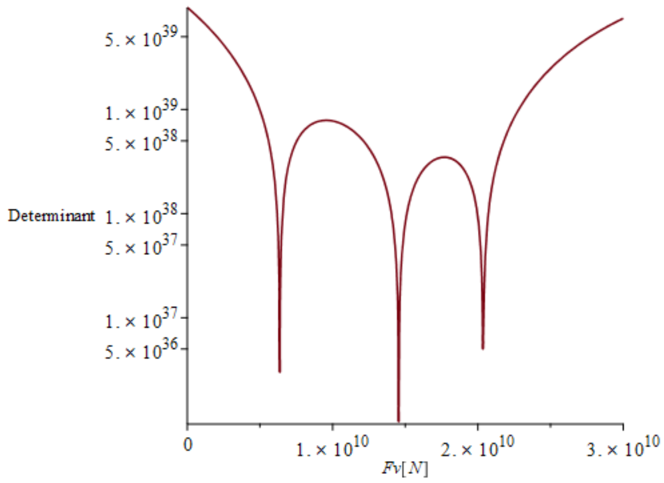

Figure 3.5: Determinant subsoil beam ($L = 28m$)

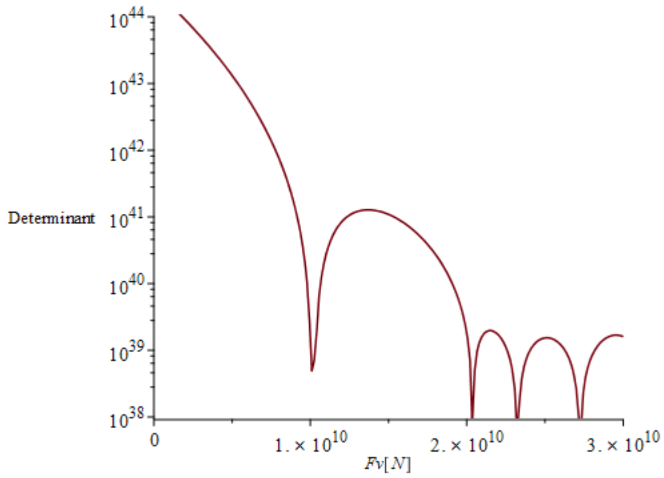

Figure 3.6: Determinant subsoil beam ($L = 100m$)

3.6. Free-free beam with axial load and partially supported by soil springs

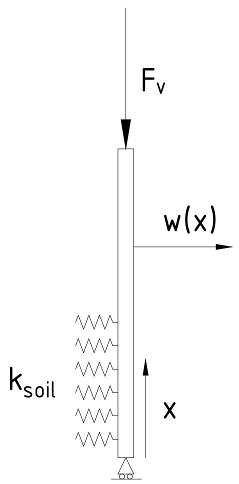

Figure 3.7: Beam model partly supported with soil springs

This model introduces interface conditions. Instead of a beam consisting of one section, two-sectioned beam is defined. These beams are connected by means of interface conditions. The lower subsoil beam is denoted by subscript 1, the upper beam is denoted by subscript 2.

For the embedded section (with the Winkler foundation), the general solution as discussed in section 3.5 is used. For the suspended section reference is made to the cantilever beam (section 3.4), or for the sake of convenience given below.

$$w_1(x) = C_{11}e^{Px}\cos(Qx) + C_{12}e^{Px}\sin(Qx) + C_{13}e^{-Px}\cos(Qx) + C_{14}e^{-Px}\sin(Qx) \tag{3.39}$$

$$w_2(x) = C_{21}cos(\alpha x) + C_{22}sin(\alpha x) + C_{23}x + C_{24} \tag{3.40}$$

With:

$$P = \sqrt{\sqrt{\frac{\beta}{4}} + \frac{\alpha}{4}} \qquad Q = \sqrt{\sqrt{\frac{\beta}{4}} - \frac{\alpha}{4}} \tag{3.41}$$

The boundary and interface conditions are given below. Note that the interface conditions are applied at $x = x_1$, which is at the seabed (for the reference model $x_1 = 28m$).

$$x = 0: \quad M_1 = 0 \quad \text{and} \quad \S_{z,1} = 0 \tag{3.42}$$
$$x = L: \quad M_2 = 0 \quad \text{and} \quad S_{z,2} = 0 \tag{3.43}$$
$$x = x_1: \quad w_1 = w_2 \quad \text{and} \quad \phi_1 = \phi_1 \tag{3.44}$$
$$M_1 = M_2 \quad \text{and} \quad S_{z,1} = S_{z,2} \tag{3.45}$$

To analyze the buckling behavior of this system, the determinant of the system of governing equation is taken. Used parameters are given in Table 3.3. The determinant of this system is plotted against the vertical force in Figure 3.8. In here, several buckling forces can be noted. Note that the order of magnitude of the buckling forces of the partly embedded pile is comparable to the buckling force of a cantilever beam (reference is made to section 3.4.

Table 3.3: Design parameters partly embedded beam

Parameter		**Unit**	**Description**
E	210	$[GPa]$	Elasticity modulus
k_{soil}	$1e8$	$[N/m^2]$	Soil stiffness
D_{pile}	6	$[m]$	Pile diameter
t_{pile}	0.06	$[m]$	Wall thickness
x_1	28	$[m]$	Penetration depth of the pile
L	132	$[m]$	Length of pile (including pen. depth)

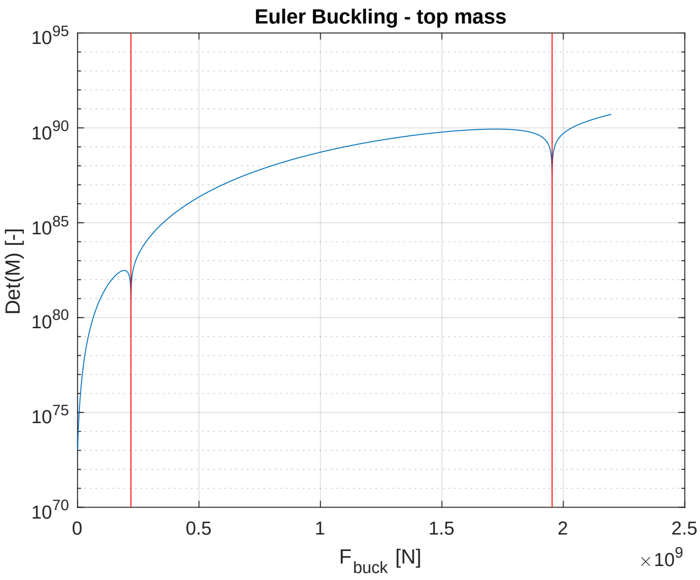

Figure 3.8: Determinant partly embedded pile

Subsequently a study is performed to analyze the sensitivity of the system to the term β, with $\beta = k_{soil}/EI$. A factor β/β_0 is introduced, where β_0 is determined with the values of Table 3.3. Note that a logaritmic scale for the x-axis is selected to visualize the inflence of the variation in β on the buckling force F_{buck}. The first buckling force as visualized in Figure 3.8 is shown with the red line.
From this figure one can conclude that the variation of β is not significantly affecting the buckling force.

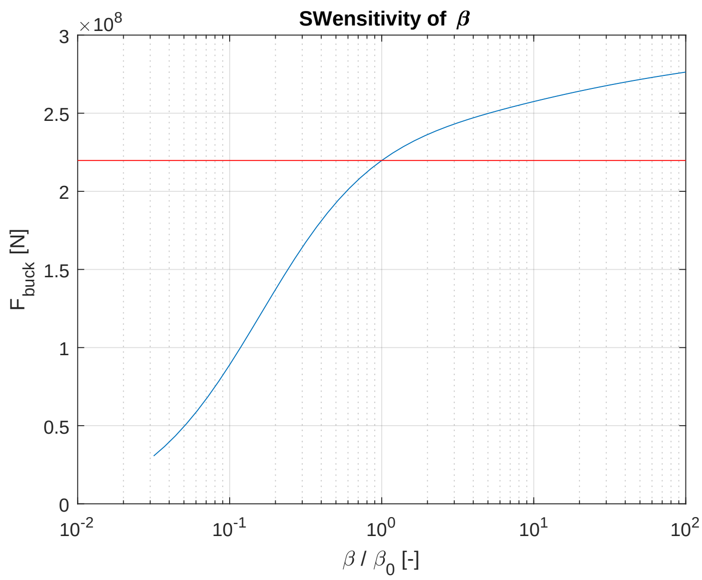

Figure 3.9: Sensitivity of β with respect to the buckling force F_{buck}

3.7. Beam model with axial- and lateral force, partly supported with soil springs

Finally, a beam with two sections is defined, including a vertical- and lateral load component. The upper section is free, the lower section is embedded in the soil, which is modeled with soil springs. A visualization of this model is given in Figure 3.10.

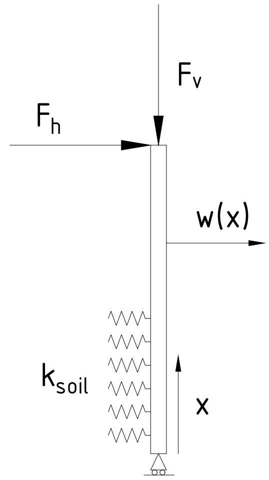

Figure 3.10: Beam model with axial- and lateral force, partly supported with soil springs

The general solutions of both the upper- and lower sections are discussed in resp. section 3.4 and section 3.5, as given below:

$$w_1(x) = C_{11}e^{Px}\cos(Qx) + C_{12}e^{Px}\sin(Qx) + C_{13}e^{-Px}\cos(Qx) + C_{14}e^{-Px}\sin(Qx) \tag{3.46}$$

$$P = \sqrt{\sqrt{\frac{\beta}{4}} + \frac{\alpha}{4}} \qquad Q = \sqrt{\sqrt{\frac{\beta}{4}} - \frac{\alpha}{4}} \tag{3.47}$$

$$w(x) = C_{21}cos(\alpha x) + C_{22}sin(\alpha x) + C_{23}x + C_{24} \tag{3.48}$$

With:

$$\alpha = \sqrt{F_v/EI} \qquad \beta = k_{soil}/EI \tag{3.49}$$

Note that in this model the cross sections remain constant over the height of the beam and the vertical force is applied at the top of the beam, and is also constant over the height of the support structure. Both ends of the structure are free, thus the boundary- and interface conditions follow as:

$$x = 0: \quad M_1 = 0 \quad \text{and} \quad \S_{z,1} = 0 \tag{3.50}$$

$$x = L: \quad M_2 = 0 \quad \text{and} \quad S_{z,2} = F_t \tag{3.51}$$

$$x = x_1: \quad w_1 = w_2 \quad \text{and} \quad \phi_1 = \phi_1 \tag{3.52}$$

$$M_1 = M_2 \quad \text{and} \quad S_{z,1} = S_{z,2} \tag{3.53}$$

Deriving the general solution to the rotation, moment and shear distributions and subsequently substituting these equations in the boundary- and interface conditions, one obtains a set of equations describing the properties of the model. A plot of the bending characteristics of this model is given in Figure 3.11. Used parameters are given in Table 3.4. Note that the maximum moment is around the seabed ($x = 28m$), which is visualized in Figure 3.11

3.8. Submerged pile

Finally, a derivation of the submerged pile is discussed. Due to loads from waves and currents, a distributed horizontal load acts on the members. This load is varies over the height of the structure, since water particle velocity increase towards the water surface. For more details on the force resulting from waves and currents, reference is made to section 4.4.4. This load distribution is simplified to be linearly decreasing from the water surface to the seabed, as shown in Figure 3.12

Since the force decreases linearly, it is assumed that the force can be mathematically expressed as follows:

$$q(x) = Ax + B \tag{3.54}$$

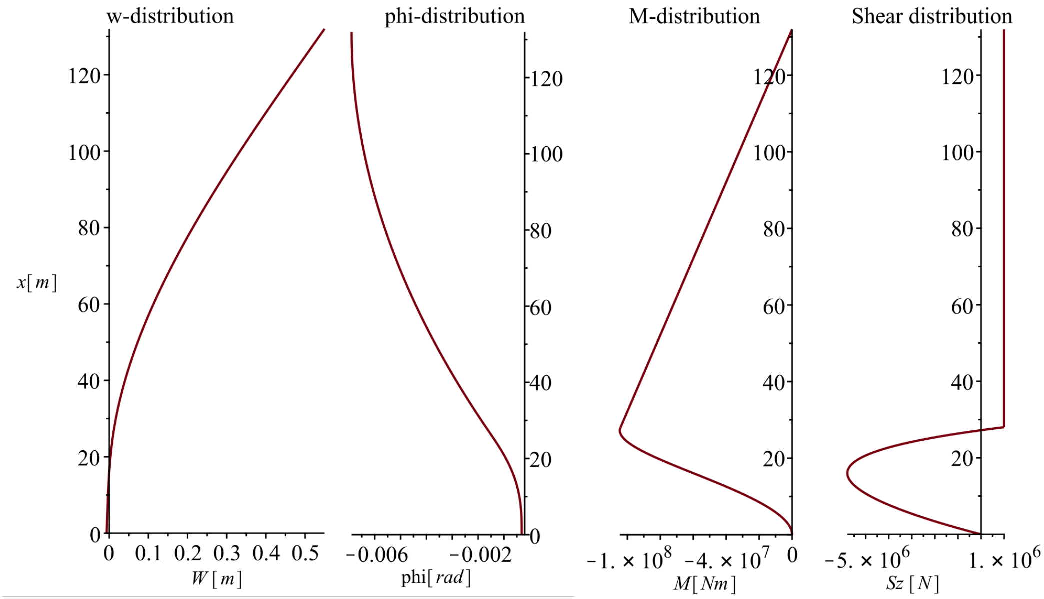

Figure 3.11: Displacement-, rotation-, moment-, and shear distribution partly embedded support structure with thrust force

Table 3.4: Design parameters cantilever beam with lateral load

Parameter		Unit	Description
E	210	$[GPa]$	Elasticity modulus
D_{pile}	6	$[m]$	Pile diameter
t_{pile}	0.06	$[m]$	Wall thickness
k_{soil}	$1e8$	$[N/m^2]$	Soil stiffness
x_1	28	$[m]$	Embedded length
L	132	$[m]$	Total length of pile
F_v	$3.5e6$	$[N]$	Vertical force (based on RNA mass)
F_t	$1e6$	$[N]$	Lateral thrust force

The governing differential equation regarding the submerged pile section is defined as:

$$\frac{d^4 w(x)}{dx^4} + \alpha^2 \frac{d^2 w(x)}{dx^2} = \frac{q(x)}{EI} \tag{3.55}$$

Where $\alpha^2 = \frac{F_v}{EI}$.

A general solution to this differential equation exists of a homogeneous- and a particular solution, resp. w_{hom} and w_{part}. w_{hom} is not different than a the dry monopile section:

$$w_{hom}(x) = C_1 \cos(\alpha x) + C_2 \sin(\alpha x) + C_3 x + C_4 \tag{3.56}$$

Subsequently the particular solution (below) is defined and tried. Note that a factor x^2 is added to obtain unique terms with respect to the homogeneous solution.

$$w_{part}(x) = (rx + s)x^2 \tag{3.57}$$

Substituting this solution in the governing differential equation gives:

$$\frac{d^4 \left(rx^3 + sx^2\right)}{dx^4} - \alpha^2 \frac{d^2 \left(rx^3 + sx^2\right)}{dx^2} = \frac{Ax + B}{EI} \tag{3.58}$$

$$0 + \frac{F_v}{EI} \frac{d^2 \left(rx^3 + sx^2\right)}{dx^2} = \frac{Ax + B}{EI} \tag{3.59}$$

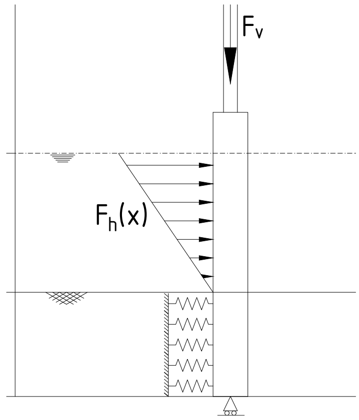

Figure 3.12: Simplied wave- and current force

Solving this equation gives the following solution (also substituting $\alpha^2 = F_v/EI$):

$$\frac{F_v}{EI}\left(\frac{rx}{6}+\frac{s}{2}\right)=\frac{Ax+B}{EI} \tag{3.60}$$

$$\frac{F_v rx}{6}+\frac{F_v s}{2}=Ax+B \tag{3.61}$$

$$r=\frac{6A}{F_v} \qquad \text{and} \qquad s=\frac{2B}{F_v} \tag{3.62}$$

Thus, the general solution can be expressed as below. Parameters A and B are obtained using the Morison equations, as discussed in section 4.4.4:

$$w(x)=C_1\cos(\alpha x)+C_2\sin(\alpha x)+C_3x+C_4+\left(\frac{6Ax}{F_v}+\frac{2B}{F_v}\right)x^2 \tag{3.63}$$

4

Final model

4.1. Introduction

A final model is defined to analyze the bending and buckling characteristics of a support structure of an offshore placed wind turbine, as visualized in Figure 4.1. This model is used to analyze research questions 3 and 4, regarding the relevance of global buckling and the second order effect in the buckling check. A beam model is derived, following from section 3. Section 5 analyzes results obtained with this final model.

4.2. Beam model

Chapter 3 discusses several beam models into depth. This theoretical framework is used to derive and discuss the final model.

The final model is built with Euler Bernouli beams, divided in 4 sections. A visualization of this beam model is given in Figure 4.1. From bottom to top, the following sections are distinguished:

1. Monopile fully embedded in Winkler Foundations.
2. Submerged monopile section. A horizontal force as result of waves and current act on the pile, increasing from the seabed to water level.
3. Dry monopile section. This section typically contains a transition piece, allowing connection between the monopile and the tower.
4. Tower section. This typically tapered section is simplified as a pile with constant diameter. On the top of this section, a horizontal thrust force is applied, as well as a vertical force representing the weight of the rotor nacelle assembly.

A uniformly distributed vertical force is applied on each section, to include the mass of the piles. Note that the vertical forces are constant over each cross-section to simplify the general solutions of the model.

4.3. Governing equations

The general form of the governing equations are given below. For details on the derivation, reference is made to section 3.

$$\begin{cases} EI_1 \frac{d^4 w_1(x)}{dx^4} + F_{v1} \frac{d^2 w_1(x)}{dx^2} + k_{soil} w_1(x) = 0, & \text{for} \quad 0 < x < x_1 \\ EI_2 \frac{d^4 w_2(x)}{dx^4} + F_{v2} \frac{d^2 w_2(x)}{dx^2} = q(x), & \text{for} \quad x_1 < x < x_2 \\ EI_3 \frac{d^4 w_3(x)}{dx^4} + F_{v3} \frac{d^2 w_3(x)}{dx^2} = 0 & \text{for} \quad x_2 < x < x_3 \\ EI_4 \frac{d^4 w_4(x)}{dx^4} + F_{v4} \frac{d^2 w_4(x)}{dx^2} = 0 & \text{for} \quad x_3 < x < L \end{cases} \tag{4.1}$$

The boundary conditions are on both the top- and bottom of the structure free-free. Or in mathematical terms:

$$x = 0: \quad M_1 = 0 \quad \text{and} \quad S_{z,1} = 0$$
$$x = L: \quad M_4 = 0 \quad \text{and} \quad S_{z,4} = -F_t$$

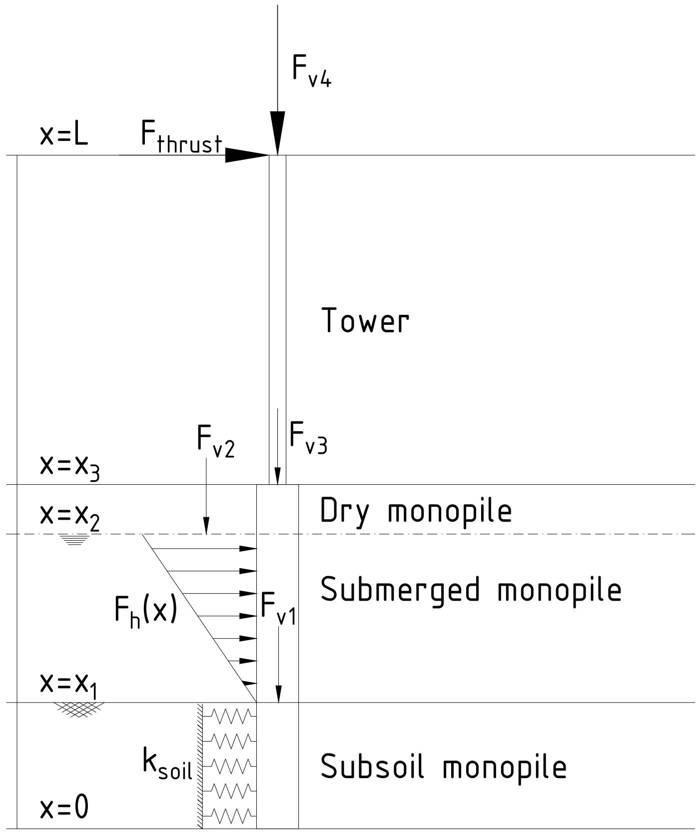

Figure 4.1: Layout analytical model wind turbine

All sections are rigidly connected to each other, without any external effects. Therefore, the interface conditions are mathematically expressed as follows:

$$x = x_n: \quad w_n = w_{n+1} \quad \text{and} \quad \phi_n = \phi_{n+1} \tag{4.2}$$

$$M_n = M_{n+1} \quad \text{and} \quad S_{z,n} = S_{z,n+1} \tag{4.3}$$

Solving the governing differential equations results in the following general solutions for the displacement of the sections:

$$w(x) = \begin{cases} w_1(x) = C_{11}e^{PX}\cos(Qx) + C_{12}e^{PX}\sin(Qx) + C_{13}e^{-PX}\cos(Qx) + C_{14}e^{-PX}\sin(Qx), & \text{for} \quad 0 < x < x_1 \\ w_2(x) = C_{21}\cos(\alpha x) + C_{22}\sin(\alpha x) + C_{23}x + C_{24} - \frac{Ax^3}{6\alpha_2} - \frac{Bx^2}{2\alpha_2}, & \text{for} \quad x_1 < x < x_2 \\ w_3(x) = C_{31}\cos(\alpha x) + C_{32}\sin(\alpha x) + C_{33}x + C_{34}, & \text{for} \quad x_2 < x < x_3 \\ w_4(x) = C_{41}\cos(\alpha x) + C_{42}\sin(\alpha x) + C_{43}x + C_{44}, & \text{for} \quad x_3 < x < L \end{cases} \tag{4.4}$$

With:

- $P = \sqrt{\sqrt{\frac{\beta}{4}} + \frac{\alpha}{4}}$
- $Q = \sqrt{\sqrt{\frac{\beta}{4}} - \frac{\alpha}{4}}$
- $\alpha_n^2 = F_{v,n}/EI_n$
- $\beta = k_{soil}/EI_1$
- $A = \frac{F_{hydro}}{EI_2(x_2 - x_1)}$
- $B = -\frac{F_{hydro}x_1}{EI_2(x_2 - x_1)}$

4.3.1. Euler buckling force

As discussed in chapter 3, the Euler buckling force of a structure can be determined by substituting the general solution of the set of equations into the boundary- and interface conditions. To ease analysis, the set of equations is to be written in matrix form (equation 4.5). All factors of the integration constants C_{11} to C_{44}, denoted as $\vec{C}$ are enclosed in matrix M. The external horizontal forces, i.e. the thrust force induced to the rotor and the wave- and current- force exerted on the wet monopile, are enclosed in vector F_h.

Note that it is required to derive the general solutions to resp. rotation $\phi(x)$, moment $M(x)$ and horizontal force $S_z(x)$, as discussed in section 3.3.

$$\underline{M}\vec{C} = \vec{F_h} \tag{4.5}$$

Where $\underline{M}$ represents the governing equations of the structure in a 16 x 16 matrix. $\vec{C}$ is a vector of the 16 integration constants $C_{11}...C_{44}$. $\vec{F_h}$ represents a vector with external load parameters. However, the stability regarding global buckling depends on the internal components only, hence the external force vector $\vec{F_h}$ is kept out of the equation.

Euler buckling occurs when the set of governing equations becomes unstable. This happens when the determinant of matrix $\underline{M}$ is equal to zero. This computation is performed using mathematical processing software Maple.

$$\det\left(\underline{M}\right) = 0 \tag{4.6}$$

Note that this computation is independent of force vector $\vec{F_h}$. The material, geometry and vertical force component are used to calculate the buckling force.

Since the vertical force component varies over the length of the pile due to the mass of the pile, a definition is given for F_{v1} to F_{v4}, as visualized in Figure 4.1.

$$F_{v4} = g(m_{top} + \eta m_4) \tag{4.7}$$

$$F_{v3} = g(m_{top} + m_4 + \eta m_3) \tag{4.8}$$

$$F_{v2} = g(m_{top} + m_4 + m_3 + \eta m_2) \tag{4.9}$$

$$F_{v1} = g(m_{top} + m_4 + m_3 + m_2 + \eta m_1) \tag{4.10}$$

With:

- m_{top} is the top mass (RNA mass)
- g is the gravitational acceleration
- η is the fraction of the pile section taken into account (elaborated on below)
- m_i the total mass of each pile section.

The mass of the pile sections apply at the top of that section. Since this mass is applied constantly over the entire section of the pile, a fraction of the pile (and thus not the entire pile) is taken into account.

Since the mass of each section is applied to the top of each section (and therefore applies to the entire section), it is chosen to factor the mass of the calculated section with η. This ensures that the vertical force taken into account is not over-conservative. To obtain insight in the buckling behavior of an offshore wind turbine, the top mass (m_{top}) is used as variable parameter.

The factor η is set to 1/3. Since the cumulative mass increases linearly over the height of a section, a triangularly shaped load shape is obtained. The center of area of this load shape is found at 1/3 from the bottom of a section: hence $\eta = 1/3$.

From the cantilever beam we learned that there are more buckling values, each corresponding to a eigenmode or buckling shape. Therefore, multiple solutions for $det(\underline{M})$ are to be expected. However, buckling will occur at the first value for the variable when the load is increased gradually, when the determinant of this matrix is equal to 0. In this case, the variable parameter is m_{top}. Figure 4.2 plots the relation between the top mass and the determinant of the system. Note that at each crossing with the horizontal axis, Euler buckling will occur.

As visualized in Figure 4.2, global buckling might occur when an RNA mass of $1.17 \cdot 10^7$ kg or larger is being applied. Reference is made to section 5 for a more elaborate analysis regarding the global buckling of this model.

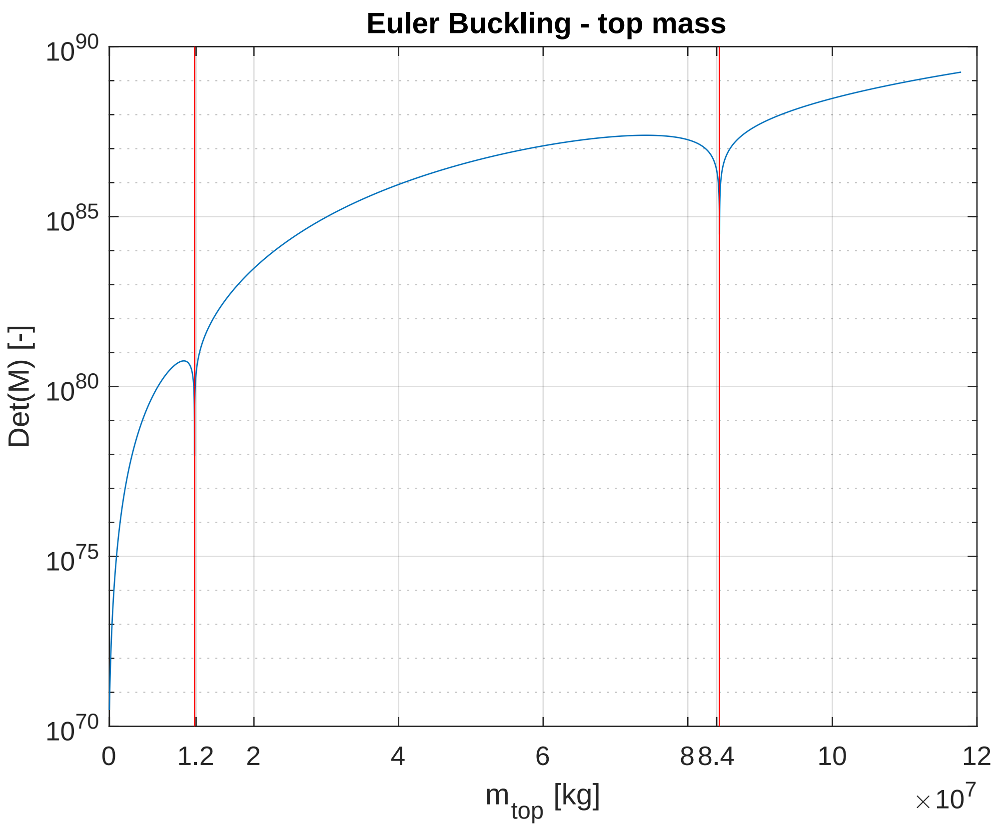

Figure 4.2: Euler buckling final model: Determinant vs m_{top}

4.3.2. Second order term

An incremental load factor is introduced to incorporate an increase in moment due to the eccentricity of the mass due to bending of the piles. This eccentricity results in a larger moment along the piles, hence in a larger deformation resulting in more eccentricity in the pile. Thus: when the displacement w increases, the moment M increases. The total moment is defined as below:

$$M_{tot}(x) = M_1(x) + M_2(x) \tag{4.11}$$

M_1 describes the moments along the pile as result of the horizontal forces. M_2, in addition, is the result of the eccentricity of the masses, distributed over the top- and along the pile.

Since the governing equations of the final model contains a second order term, the incremental load factor is accounted for.

To determine the magnitude of the second order moment, equation 4.11 is rewritten:

$$M_2(x) = M_{tot}(x) - M_1(x) \tag{4.12}$$

Note that the total moment is defined by the final model including all vertical loads, where M_1 is obtained by neglecting these vertical forces. The system of equations to obtain M_1 becomes:

$$\begin{cases} EI_1 \frac{d^4 w_1(x)}{dx^4} + k_{soil} w_1(x) = 0, & \text{for} \quad 0 < x < x_1 \\ EI_2 \frac{d^4 w_2(x)}{dx^4} = q(x), & \text{for} \quad x_1 < x < x_2 \\ EI_3 \frac{d^4 w_3(x)}{dx^4} = 0, & \text{for} \quad x_2 < x < x_3 \\ EI_4 \frac{d^4 w_4(x)}{dx^4} = 0, & \text{for} \quad x_3 < x < L \end{cases} \tag{4.13}$$

Solving these ordinary differential equations provide us with the following general solution:

$$w_1(x) = \begin{cases} w_1(x) = C_{11}e^{-\beta x}\cos(\beta x) + C_{12}e^{-\beta x}\sin(\beta x) + C_{13}e^{\beta x}\cos(\beta x) + C_{14}e^{\beta x}\sin(\beta x), & \text{for} \quad 0 < x < x_1 \\ w_2(x) = C_{21}x^3 + C_{22}x^2 + C_{23}x + C_{24}+, & \text{for} \quad x_1 < x < x_2 \\ w_3(x) = C_{31}x^3 + C_{32}x^2 + C_{33}x + C_{34}, & \text{for} \quad x_2 < x < x_3 \\ w_4(x) = C_{41}x^3 + C_{42}x^2 + C_{43}x + C_{44}, & \text{for} \quad x_3 < x < L \end{cases} \tag{4.14}$$

In section 5 the effect of this second order moment is analyzed and discussed.

4.4. Parameters

4.4.1. Monopile sections

The substructure is divided in 4 sections, see figure 4.1 for a visualization of the sections. Below the sections are listed from top to bottom:

- Tower
- Dry monopile
- Submerged monopile
- Subsoil monopile

Several parameters are simplified to allow fast analysis of the model. For example, diameters and wall thicknesses of each sections are modeled as being constant over the length of the section. The elasticity modulus and density of steel used troughout this thesis are given below. Note that the density of steel is adjusted to account for internal components such as internal cables and the other equipment installed inside the pile.

- $E = 210GPa$
- $\rho_{steel} = 8500kg/m^3$

The moment of inertia (I) and the cross sectional area (A) for a round tubular section is calculated below:

$$I = \frac{\pi}{64}(D_o^4 - D_i^4) \qquad A = \frac{\pi}{4}(D_o^2 - D_i^2) \tag{4.15}$$

Where D_o and D_i are resp. the outer- and inner diameter of the pile, where the inner diameter is dependent on the wall thickness t.
A distribution of the diameter- and thickness of the support structure of the reference turbine are given in Figure 4.3. Quantification of the parameters regarding the reference model are given in table 4.1.

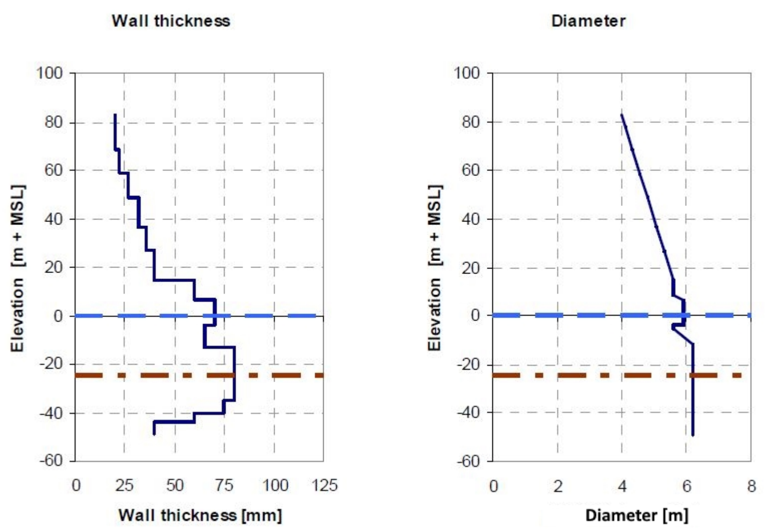

Figure 4.3: Diameter- and wall thickness distribution reference model

Table 4.1: Parameters reference model

Parameter	**Unit**	**Subsoil**	**Submerged**	**Dry Monopile**	**Tower**
x_{lower}	m	0	$x_1 = 28$	$x_2 = 50$	$x_3 = 60$
x_{upper}	m	$x_1 = 28$	$x_2 = 50$	$x_3 = 60$	$L = 142$
D_o	m	6.1	6.1	5.75	5.0
wt	mm	75	60	60	30
I	m^4	6.44	5.2	4.34	1.45
A	m^2	1.42	1.13	1.07	0.47

4.4.2. Soil stiffness

For this model linear soil springs are used to simulate the soil-pile interaction. One method to determine this soil stiffness is to use so called p-y curves. These curves visualize the relation between the lateral pile displacement and the soil pressure by means of the following expression:

$$k_{soil,py} = \frac{p_i}{y} \tag{4.16}$$

Where $k_{soil,py}$ is the soil stiffness, y is the lateral displacement of the pile and p_i is the soil pressure (see expression below). Note that this method is applicable for sandy soils only.

$$p_i = Ap_u \tanh\left(\frac{k_s H y}{A p_u}\right) \tag{4.17}$$

$$p_u = (0.115 \cdot 10^{0.0405\phi} z + 0.571\dot{1}0^{0.0555\phi} D)\sigma_v \tag{4.18}$$

$$k_s = (0.008085\phi^{2.45} - 26.09)10^3 \tag{4.19}$$

With:

- A is the factor for static- or cyclic loading (0.9 throughout this thesis).
- H is the depth
- y is the lateral displacement
- ϕ as internal friction angle. This method is relevant for $29 \leq \phi \leq 45$.
- σ_v is the effective vertical stress at the considered depth.

Pressure in the soil σ_v is calculated at the relevant relevant depth in the soil, including the weight of the water column and the soil:

$$\sigma_v = g(h_{water}\rho_{water} + h_{soil}\rho_{soil} \tag{4.20}$$

Throughout this thesis the following values are applied, unless mentioned differently:

- g is the gravity, $9,81 m/s^2$ on this planet;
- ρ_{water} is the density of seawater ($1025 kg/m^3$);
- h_{soil} is the reference depth of the soil stiffness. Taken as $9m$;
- ρ_{soil} is the soil density, taken as $1010 kg/m^3$ [11]

Table 4.2: Parameter definition soil types

Soil types	H $[m]$	A $[-]$	ϕ**[11]** $[deg.]$	σ_v $[kPa]$	k_{py} $[N/m^3]$
Loose sand	28	0,9	29	318	$1,01e8$
Medium sand	28	0,9	33	318	$1,66e8$
Dense sand	28	0,9	38	318	$2,45e8$

4.4.3. Thrust force

Wind powers the rotor to rotate, which is used to drive the the generator in the hub of the wind turbine. To control the power that is generated by means of the blades, a blade-pitch system is installed. This system rotates the blades to a certain angle to ensure both the integrity of the structure and the power production. Figure 4.4 visualizes this pitch angle. On the left a low pitch angle is set to ensure the blade is as flat as possible. However, when the wind speed increases, the pitch angle is increased, resulting in a smaller frontal surface of the blade. This also results in a lower lateral force on the tower.

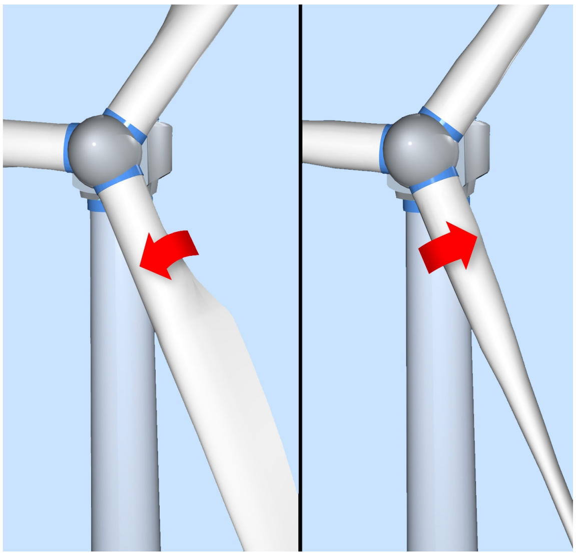

Figure 4.4: Blade pitch (left: wind up to rated wind speed, right: wind exceeding rated wind speed)

Due to this control system, the maximum thrust force is reached at the rated wind speed. At this wind speed, the maximum power the generator can handle is used, but the blade is still pitched minimally. For the reference model this results in a maximal thrust force F_t of 1000 kN. Note that this load is static. Due to propagating eddies the wind speed may locally exceed the rated wind speed. Since the pitch system can not react on these eddies, the total thrust force might be slightly higher.

4.4.4. Hydrostatic force

Waves and currents are flowing around the monopile of the wind turbine. These flows result in a hydrostatic force that acts on the monopile. However, to allow the model to be analyzed analytically, the force is determined to be linearly decreasing: At mean sea level the force is considered maximal, where at the seabed the force is considered to be 0. The force distribution is schematically shown in Figure 3.12

The hydrostatic force $q(x)$ force is defined in equation (ref equation below)

$$q(x) = F_h \frac{x - x_1}{x_2 - x_1} \tag{4.21}$$

Where x_1 and x_2 describe elevations for resp. the seabed and water level. F_h is a factor that describes the maximum force, acting at mean sea level on the pile, calculated using the Morison equation:

$$F_{morison} = \frac{\pi}{4} D^2 \rho_{water} C_m \dot{u} + \frac{1}{2} C_d \rho_{water} D u|u| \tag{4.22}$$

where D is the diameter of the pile,C_m and C_d are resp. the inertia- and drag coefficient, ρ_{water} is the density of water and u and $\dot{u}$ are resp. the water particle velocity and acceleration. Typical values for inertia- and drag coefficient C_m and C_d are resp. 0.7 [15] and 2.0 [15].

The water particle velocity is typically a combination of the current speed and the wave speed. The maximum wave velocity and acceleration are determined using Airy theory. Based on orbital motions of the water particles in the wave, an expression is formed for the maximum particle velocity.

$$u = u_{current} + u_{wave} \tag{4.23}$$

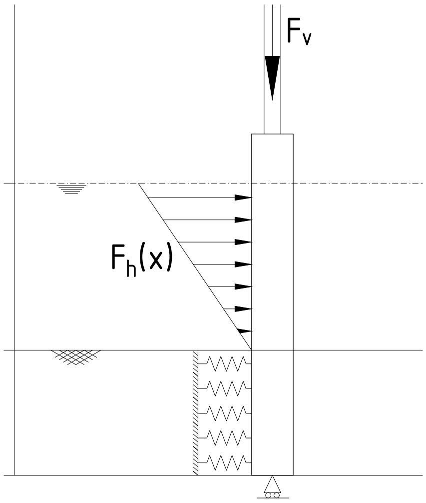

Figure 4.5: Simplied hydrostatic force

$$u_{wave} = \zeta \omega e^{kz} \tag{4.24}$$

$$\dot{u}_{wave} = \zeta \omega^2 e^{kz} \tag{4.25}$$

Where ζ is the wave amplitude, ω is the wave frequency, k is the wave number and z is the vertical location of the water particle. When the water particle velocity expression is derived with respect to time, we obtain the particle acceleration term [9]. The maximum wave velocity and acceleration is reached at $z = 0$, the top of the wave.

Note that the values for the required parameters are dependent on the limit state that is checked. For example, when an ultimate limit state (ULS) is tested, a wave that exists once every 50 years is used to determine the hydrostatic loads. Also note that these hydrostatic forces are simplified by taking the maximum wave velocity- and acceleration at mean sea level, where actually the wave exceeds this level. This is compensated by decreasing the force over height linearly instead of quadratically.

Parameters for the hydrostatic load regarding the reference model are given in Table 4.3.

Table 4.3: Hydrostatic load

Parameter	**Value**	**Unit**	**Parameter**	**Value**	**Unit**
$u_{current}$	1.5	m/s	ζ	17.48	m
C_d	0.7	$-$	ω	0.578	rad/s
C_m	2.0	$-$	$u_{wavemax}$	10.1	m/s
ρ_{water}	1020	kg/m^3	$\dot{u}_{wavemax}$	5.84	m/s^2
D	6.1	m	F_h	406	kN/m

5 Analysis

5.1. Introduction

This chapter elaborates on the analysis of the final model and elaborates on- and discusses the results, keeping the research questions in mind. Firstly the buckling length comes to order. How can a buckling length be chosen for a preliminary buckling check? Subsequently the second order effect is analyzed, referring to the second order term in the governing differential equations of the beam models. Finally, a case- and sensitivity study is carried out, analyzing the relevance of several parameters and also comparing the local buckling check to the global buckling check.

5.2. Buckling length

The Euler buckling force is defined as per equation 5.1. In this section a definition is sought for the buckling length L_{buck} (ref. equation 5.2.

$$F_{buck} = \frac{\pi^2 EI}{L_{buck}^2} \tag{5.1}$$

$$L_{buck} = \sqrt{\frac{\pi^2 EI}{F_{buck}}} \tag{5.2}$$

However, a monopile based offshore wind turbine is not clamped at the bottom, nor is the geometry constant over the height of the structure. Therefore, the buckling length is approached from two angles:

- The varying geometry, inclined at the seabed
- Boundary condition at the seabed: what influence has the soil on the buckling length?

5.2.1. Varying geometry

In this section a buckling length L_{buck} is determined. This length is calculated using the following equation:

$$L_{buck}(x) = \sqrt{\frac{\pi^2 EI(x)}{F_{buck}}} \tag{5.3}$$

However, note that the stiffness term $EI(x)$ is dependent the geometry, and thus on the height of the pile. Reference is made to Figure 5.1 for a visualization of the varying diameter- and wall thickness of the base case as discussed in section 4.
Assuming that the buckling force is a constant, the bucklnig length must vary over the height of the structure with a non-constant stiffness term (referring to equation 5.3). To obtain a buckling length, constant over the length of the structure, a constant stiffness term needs to be obtained.

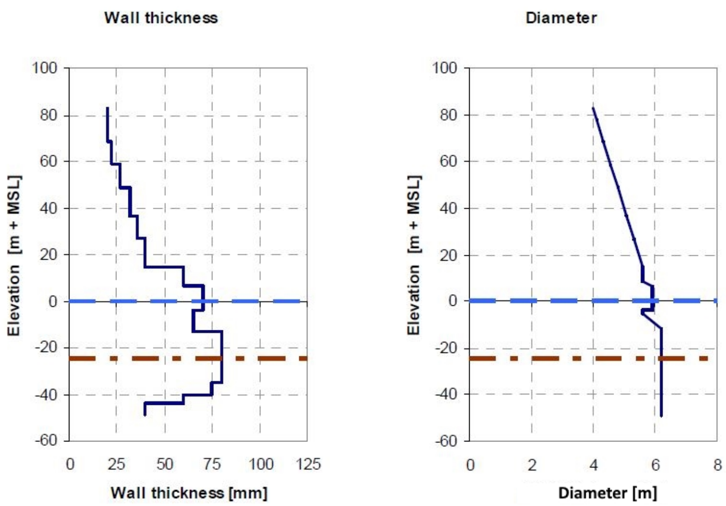

Figure 5.1: Diameter- and wall thickness distribution reference model

This constant stiffness term EI is determined by computing the displacement of the rotor nacelle assembly using the model and parameters as discussed in section 4, as per reference model. This displacement is subsequently used to determine a value of the stiffness term, which is used to calculate a buckling length. The used loadcase and obtained displacement are enlisted below. Note that for this study both water forces and tower/pile drag are neglected.

A stiffness term EI is determined, using rules of thumb for a cantilever beam [19]. Note that the values used below follow from the final model as discussed in 4.

$$\delta_{max} = \frac{FL^3}{3EI} \qquad \rightarrow \qquad EI = \frac{FL^3}{3\delta_{max}} \tag{5.4}$$

$$EI = \frac{1e6 \cdot 104^3}{3 \cdot 0,717} = 5.2e11[Nm^2] \tag{5.5}$$

With:

- EI is the flexural stiffness term, independent of height x
- δ_{max} is the maximum displacement at the top of the structure
- L is the length of the support structure from seabed to RNA
- F is the lateral load, induced by the wind on the RNA

The buckling length of the reference turbine follows from equation 5.3. Since we determined the buckling force in section 4.3.1 using the final model, one can enter the following expression and conclude the buckling length:

$$L_{buck} = \sqrt{\frac{\pi^2 EI}{F_{buck}}} = \sqrt{\frac{\pi^2 5.2e11}{1.3e8}} = 228[m] \tag{5.6}$$

228 meter is a factor 2,2 higher than the actual length of 104 meter (from seabed to RNA). Note that this factor is even higher than the factor 2 which corresponds to the buckling length of a cantilever beam, as visualized in Figure 1.6.

5.2.2. Foundation

To determine what the effects of the foundation-pile interaction is on the buckling length of a monopile, a set of soil conditions is defined. Reference is made to section 4.4.2 where the modeling of the pile-foundation interaction is discussed.

Three soil types are distinguished in this thesis. Also the penetration depth of the soil is taken into account, resulting in the loadcases presented in Table 5.1. Note that both the soil type and the penetration depth vary in the loadcases. Reference is made to section 4.4.2 for more details on the different parameters.

Table 5.1: Loadcases buckling length soil stiffness

Loadcase	**Soil types**	H $[m]$	A $[-]$	ϕ $[deg.]$	σ_v $[kPa]$	k_{py} $[N/m^3]$
1.	Loose sand	28	0,9	29	318	$1,01e8$
2.	Medium sand	28	0,9	33	318	$1,6e8$
3.	Dense sand	28	0,9	39	318	$1,3e8$
4.	Medium	15	0,9	33	318	$1,6e8$
5.	Medium	50	0,9	33	318	$1,6e8$

Now the influence of the buckling length is being determined. As in section 5.2.1, the buckling length is determined using equation 5.4. Note that the same (constant) flexural stiffness EI is being used as in section 5.2.1.

Table 5.2: Buckling length: soil conditions

Loadcase	**Soil types**	H $[m]$	L_{buck} $[m]$
1.	Loose sand	28	211,75
2.	Medium sand	28	210,00
3.	Dense sand	28	209,10
4.	Medium	15	239,38
5.	Medium	50	209,75

The various buckling lengths as result of the different soil stiffness's and penetration depths are given in Table 5.2. Here it can be noted that the influence of the foundation parameters does influence the buckling length.

A loose soil stiffness results in a longer buckling length than a more dense variation of the soil. This can be explained by means of the buckling shape of the structure. When a shape is inclined at one side and free at the other side, the buckling shape can be mirrored, and the buckling length is taken as twice the length of the pile. A visualization of the buckling length is enclosed in Figure 5.2 Here, however, we have a non-inclined boundary condition. Therefore the buckling shape of the pile is angled at the seabed and the buckling length is different.
To verify whether the findings were plausible, the soil stiffness was increased, approaching infinity, resulting in a buckling length of twice the length, equal to a cantilever beam.

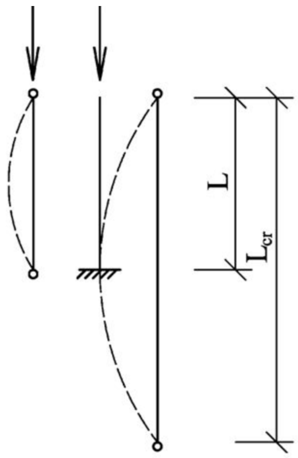

Figure 5.2: Buckling length of a cantilever beam

Regarding the penetration depth of the pile, the same effect is noticed as with the soil stiffness variation. A larger penetration depth stiffens the structure, which leads to a shorter buckling length. However, when the penetration depth is lengthened to infinity, a buckling length is obtained that is larger than for a cantilever beam. This is explained by the buckling shape: at the seabed the pile is not vertical, hence the buckling shape, and therefore the buckling length is longer. A visualization of the deformation shapes is given in Figure 5.3.

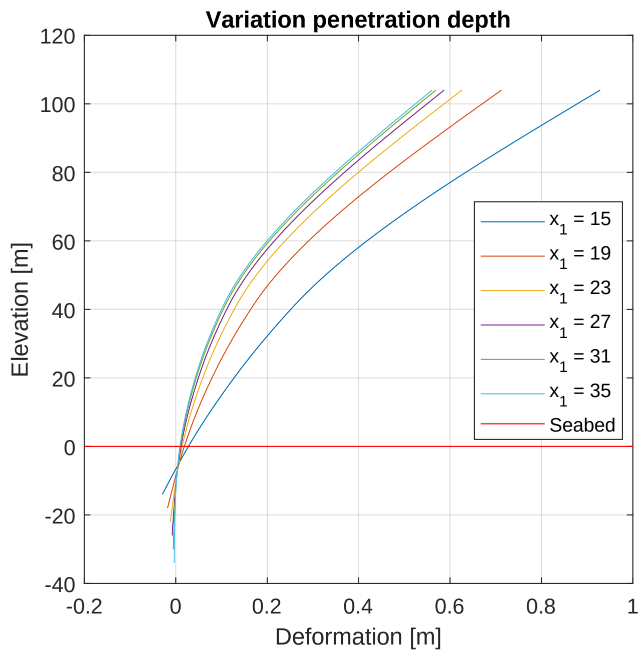

Figure 5.3: Sensitivity penetration depth:deformation curves

5.3. Second order term

The set of ordinary differential equations describing the model as discussed in section 4 (for convenience given below), consists of 4 differential equations, each containing a second order derivative. This second order term describes the influence of the vertical load on the displacement of the structure. The influence of this second order term will be analyzed and discussed in the sections below.

5.3.1. Base case study

The final model as discussed in chapter 4 gives a set of ordinary differential equations, including a second order term. However, section 4.3.2 discusses a derivation of the same model, withou a second order term. Figure 5.4 visualizes the differences in displacement, rotation, moment and shear force over the height of the structure.

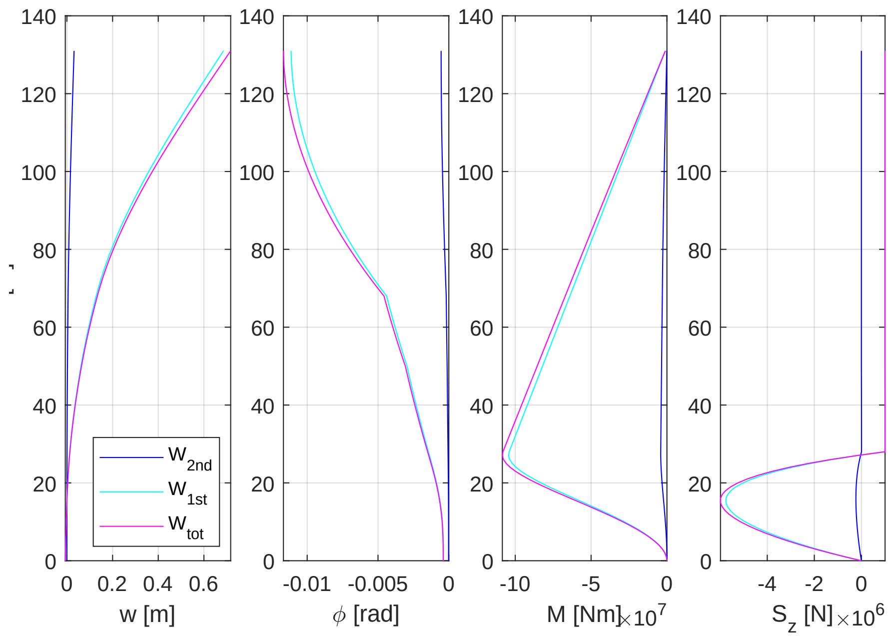

Figure 5.4: Euler buckling final model: Determinant vs m_{top}

In these figures it can clearly be seen that the influence of the second order term (given in blue), is much smaller than the results of the “first” order term (given in cyan). Figure 5.5 gives the percentage that the 2nd order term contributes to the total of the displacement, rotation, moment and shear force.
Figure 5.5 provides a visualization of the effect the second order term has on the total amount of deformation, rotation, moment and shear force. The total value is divided by the contribution of the second order. For example, the moment is determined as follows. Note that the used parameters are based on the reference turbine.

$$M_{frac} = \frac{M_{2nd}(x)}{M_{total}(x)} \tag{5.7}$$

The second order term affects the mechanical properties of the structure minimally. Approximately 4,5% is the contribution of this term. However, this does not mean that the term may or should be neglected when checking for global buckling. Reference is made to section 5.3.2 where an incremental load factor is introduced.

5.3.2. Incremental load factor (ILF)

An incremental load factor (ILF) might be beneficial to introduce to allow first order analysis regarding buckling of a monopile based offshore wind turbine. Figure 5.6

The ILF that is introduced is based on the moment lines of the reference turbine, as calculated per chapter 4, as given below:

$$ILF = 1 + \frac{M_{2nd}(x)}{M_{1st}(x)} \tag{5.8}$$

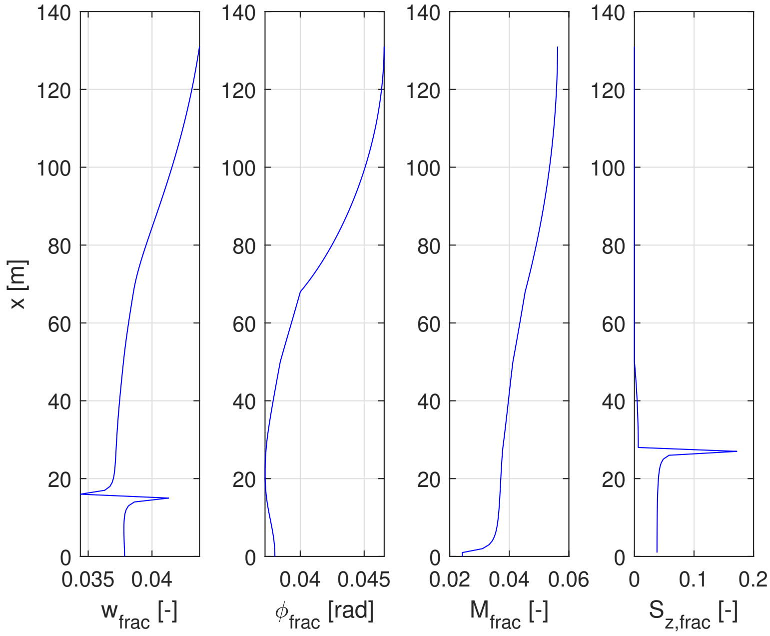

Figure 5.5: Fraction second order term versus total. Left to right: displacement-, rotation-, moment- and shear distribution.

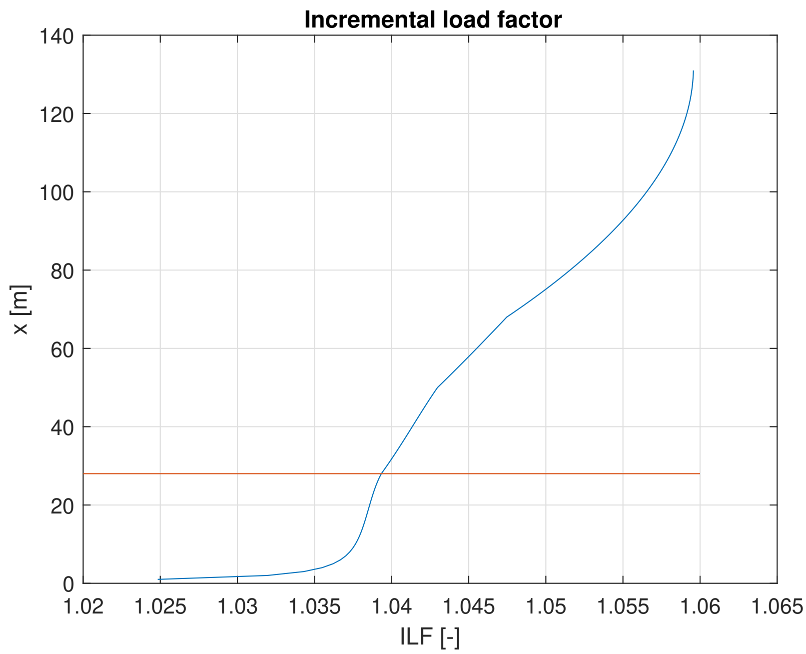

Figure 5.6: Incremental load factor over the height of the pile

An ILF may could be used in the design of an offshore wind turbine.

- Reduce the ILF to a single value for the entire structure. Referring to Figure 5.6, 1.055 would be a rather conservative value.
- Perform a first order analysis, as per paragraph 4.3.2. Both the moment, shear force and the displacement should be factored by the ILF.
- Perform the required checks as prescribed by the design standards. For example the global buckling check as described by the Eurocode.

- Review the design and its parameters to optimize the design.

In this manner, an optimized design can be obtained without using a model based on second order terms. This may be beneficial for designers

5.4. Sensitivity study

In this section several parameters are discussed on sensitivity, regarding global buckling of a monopile based offshore wind turbine. The following parameters affect the buckling strength of the structure directly, since they affect the Euler Buckling equation and are therefore analyzed for sensitivity:

- Soil type and penetration depth
- Pile diameter and wall thickness

5.4.1. Soil type and penetration depth

The soil stiffness and the penetration depth affect the buckling behavior of a structure. The foundation functions as a boundary condition, which is exceeded over a length of the structure. To visualize the influence of these parameters, the final model is being used. In short: the stability of the structure is analyzed by computing the different segments analytically. These segments, including the boundary- and interface conditions are rewritten as a matrix equation ($\underline{M}\vec{C} = \vec{F}_h$).

Regarding the soil stiffness, a range of quantities is selected based on occurring scenarios. Different types of sand are taken into account, ranging from very loose to very dense. Also the penetration depth is quantified according to realistic values. A visualization of both sensitivity curves is given in Figure 5.7.

The values of the soil stiffness are based on very loose sand [11] up to a rigidly connected structure. Reference is made to section 5.2.2 for relevant calculations of the soil stiffness.

A penetration depth of 8 meter is chosen to be as the lower level. From here, it is chosen to increase the depth up to 40 meter, from where the buckling behavior is expected not to change any further.

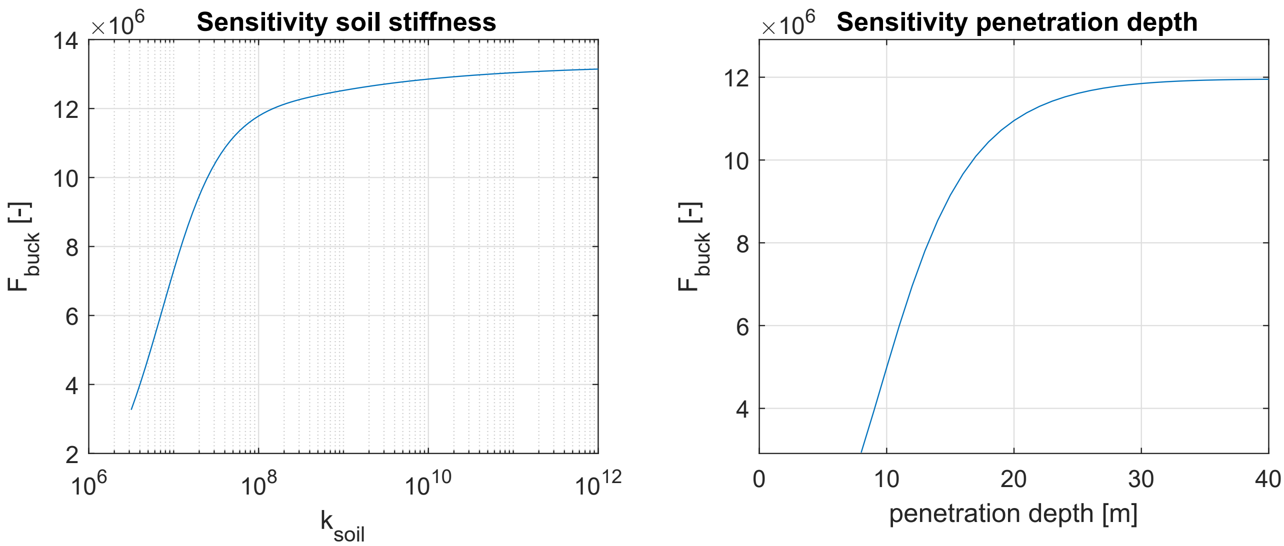

Figure 5.7: Buckling sensitivity soil stiffness and penetration depth

An increase in soil stiffness results in an increase in global buckling resistance. The maximum buckling resistance increases to the buckling resistance where the lower boundary condition is rigidly connected in the seabed (equal as a cantilever beam).

5.4.2. Pile diameter and wall thickness

Flexural stiffness (EI) is a term used directly in the Euler Buckling equation. This value consists of the Elasticity modulus E, and the inertia term I. This latter term is dependent on the cross sectional dimensions of the structure, in this case the diameter D and wall thickness t. The ratio between these values (D/t ratio), is a major parameter in buckling analysis in general, since it obtains insight the sensitivity to shell buckling in one simple expression. Therefore it is chosen to use the D/t ratio as a tool to analyze the global buckling behavior of a monopile based wind turbine.

For this paragraph, the cross sectional area A is kept constant and the diameter is changed. In this manner the wall thickness is decreased, when the diameter increases.

$$A = \frac{1}{4}\pi\left(D^2 - (D-2t)^2\right) \tag{5.9}$$

Where D is the outer diameter and t is the wall thickness of the pile.

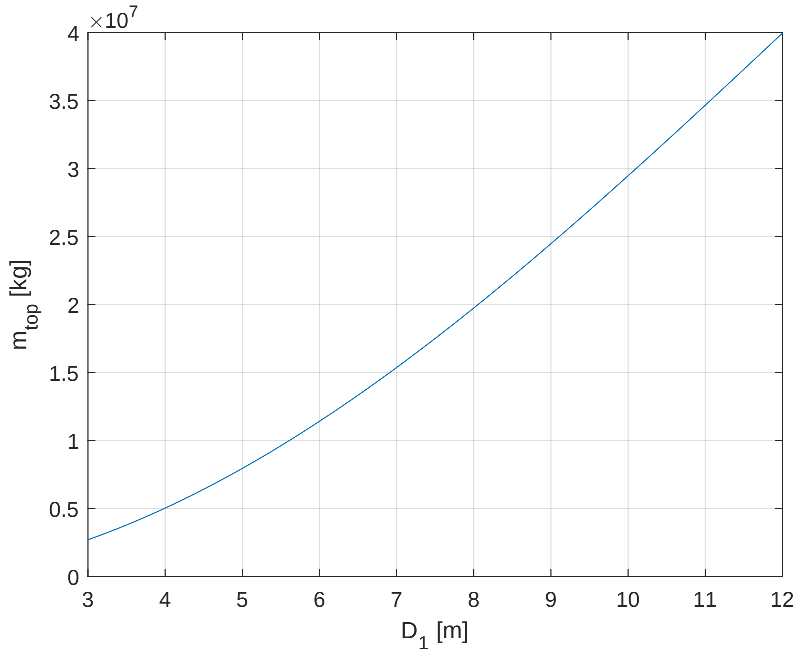

Figure 5.8: Buckling sensitivity D/t ratio

Here it can be noted that the influence of the pile diameter and thickness influences the buckling resistance significantly. This is expected, since the diameter term is present in the inertia term which subsequently is used in the Euler buckling equation.

However, even for the lower diameter piles, relevance regarding global buckling may be disputable, referring to the mass of the reference wind turbine is determined to be 350.000 kg [8]. From Figure 5.8 it can be concluded that at an outer diameter of 3 meter, the RNA would be required to have a mass of 2.700.000 kg. This is approximately a factor 7,5 larger than the designed mass of the RNA, where the diameter of 3 meter also is unrealistic small. Also note that the required buckling mass at a more realistic diameter of 6 meter is around 11.400.000 kg, which is over a factor 32 higher than the design mass.

Furthermore it should be taken into account that global buckling might be irrelevant for these values of the diameter and wall thickness, however, regarding other failure modes, such as local buckling, it might be very relevant. In this paragraph the wall thickness decreases when the diameter increases, making it more sensible for imperfections such as locally concentrated stresses. Section 5.5.2 elaborates on the relevance of local buckling regarding global buckling.

5.5. Case study

This section elaborates further on the standards as discussed in chapter 2. Firstly, in section 5.5.1 a comparison of the buckling checks as per Eurocode and DNVGL is discussed. Are there significant differences, and if yes, where do they originate?

Subsequently the local buckling check of the Eurocode is compared to the global buckling check of the Eurocode. With this comparison the relevance of the global buckling check with respect to the local buckling check is discussed.

5.5.1. Global buckling check comparison: Eurocode versus DNVGL

Two global buckling checks are applied and compared: the Eurocode [5] and the DNVGL [3]. Both checks are applied on the reference model, as discussed in chapter 4. The protocol of the checks are discussed in chapter 2. Both buckling checks are given in the equations below. Equation 5.10 describes the check for the Eurocode, equation 5.11 describes the buckling check for the DNVGL. However, since these checks take non-axial forces into account, the term global buckling is not strictly correct. Global buckling, as Leonhard Euler described it [14] is initiated by axial forces only.

$$\frac{N_{Ed}}{\frac{\chi_y N_{Rk}}{\gamma_{M1}}} + k_{zy}\frac{M_{y,Ed} + \Delta M_{y,Ed}}{\frac{\chi_{LT} M_{y,Rk}}{\gamma_{M1}}} + k_{zz}\frac{M_{z,Ed} + \Delta M_{z,Ed}}{\frac{M_{z,Rk}}{\gamma_{M1}}} \leq 1 \tag{5.10}$$

$$\frac{N_d}{\kappa N_p} + \frac{\beta_m M_d}{M_p} + \Delta N \leq 1 \tag{5.11}$$

Both checks consist of a summation of several parameters, which should be smaller or equal to 1. When this unity check is not satisfied, failure will occur. However, the check as per Eurocode seems more complicated than the DNVGLs check. This is relative, since both checks require some effort to define the non-moment and non-compression terms. Besides that, the resistance- and design parameters (normal forces and moments) are comparable. Furthermore, the Eurocode takes torsion into these equations, which are neglected throughout this thesis, and thus this comparison.

It is recommended to review both standards for a complete view of the protocol [5] [3]. However, reference is made to chapter 2 for a short summary of the relevant sections of these standards.

Regarding the normal force, the Eurocode introduces a term χ_x where the DNVGL introduces κ. Both these terms are related to the global buckling effect: the sensitivity regarding global buckling is expressed in these flexural buckling coefficient.
Regarding the moment term, however, another coefficient is introduced. The DNVGL uses the moment factor β_m where the Eurocode introduces the term interaction factor k_{yy}. Both terms take the slenderness of the structure into account in this term.

Finally the DNVGL introduces one more slenderness parameter: ΔN. This term is used as extra safety factor.
Both checks are filled in and compared. To do so, the most sensitive spot of the pile is to be selected: The normal force and the bending moment are taken on this spot, allowing for a high as possible unity check. To find this section on the pile, the normal-and moment distributions of the model are analyzed, as given in Figure 5.9.

In these distributions it can be seen that the maximum moment and the normal force distribution are maximum around the seabed. Therefore it is chosen to perform the buckling checks at the seabed.

The results of these checks are as follows:

- Global buckling check DNVGL: $0,0438 \leq 1$;
- Global buckling check Eurocode: $0,022 \leq 1$.

It can be noted that these checks point out that buckling will not be an issue for the reference wind turbine. Since the values are resp. a factor 22 and 44 lower, it can be considered that this check is less relevant for comparable support structures. However, since a trend of larger wind turbines in deeper seas and in a variety of soil types is noted, one can consider that these checks might become relevant for these turbines.

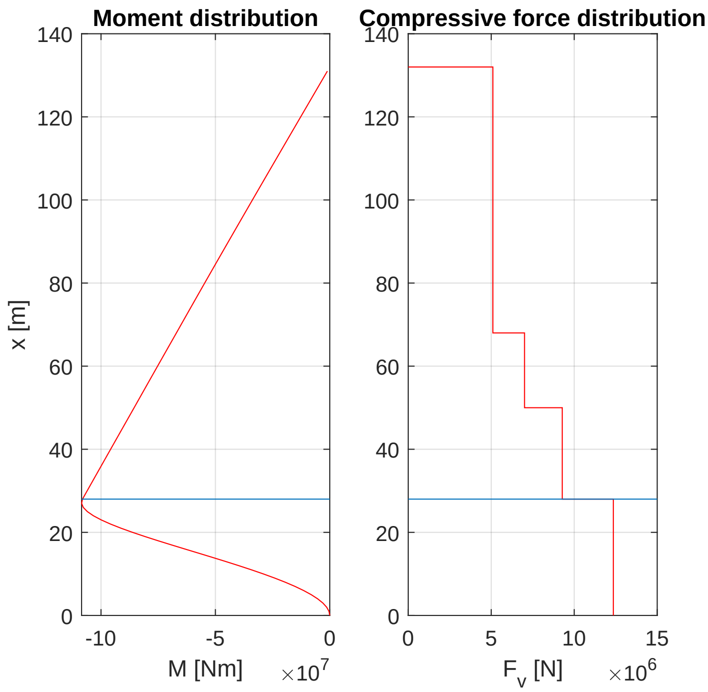

Figure 5.9: Normal force- and moment distribution (red), seabed (blue)

5.5.2. Global buckling check versus local buckling check: Eurocode

In this section Eurocode's global buckling check is compared to its local buckling check. This is done using the parameters of the reference turbine as input. Firstly, reference is made to chapter 2 for a summary of both the local and global buckling check. The equations below are the main equations of these checks. Firstly the global buckling check is given (equation 5.12). Subsequently, the local buckling check is given (equation 5.13.

$$\frac{N_{Ed}}{\frac{\chi_y N_{Rk}}{\gamma_{M1}}} + k_{zy}\frac{M_{y,Ed} + \Delta M_{y,Ed}}{\frac{\chi_{LT} M_{y,Rk}}{\gamma_{M1}}} + k_{zz}\frac{M_{z,Ed} + \Delta M_{z,Ed}}{\frac{M_{z,Rk}}{\gamma_{M1}}} \leq 1 \tag{5.12}$$

$$\left(\frac{\sigma_{x,Ed}}{\sigma_{x,Rd}}\right)^{k_x} + k_i\left(\frac{\sigma_{x,Ed}}{\sigma_{x,Rd}}\right)\left(\frac{\sigma_{\theta,Ed}}{\sigma_{\theta,Rd}}\right) + \left(\frac{\sigma_{\theta,Ed}}{\sigma_{\theta,Rd}}\right)^{k_\theta} + \left(\frac{\tau_{x\theta,Ed}}{\tau_{x\theta,Rd}}\right)^{k_\tau} \leq 1 \tag{5.13}$$

Note that the global buckling check has its focus on normal forces and moments, where the local buckling check takes stresses into account. The elevation where these checks are taken is on seabed level.

- Global buckling check Eurocode: $0,022 \leq 1$;
- Local buckling check Eurocode: $0,049 \leq 1$.

The local buckling check scores higher on the unity check, meaning that it is closer to failing locally than globally, and therefore more relevant for the reference wind turbine. However, note that these are two different check, which may always be relevant for the design of a support structure of an offshore wind turbine, especially when the dimensions of the RNA, mean sea level, soil conditions and other parameters are different for every different wind turbine. Since the trend is to have larger structures offshore, it is interesting to see how these new designs affect these buckling checks.

Note that the differences in result between the Eurocode and the DNVGL is over a factor 2, which may be considered quite high. Reference is made to section 2.5, where it is stated that the DNVGL is likely to be more concervative than the Eurocode, since the Eurocode goes more into depth. However, the offset in results may also be declared regarding the range of the solution. The global buckling check is a unity check, resulting in a failure- or non-failure. Therefore the accuracy of this test should be highest around the bifurcation point of failure. However, since the results of the tests conducted in this thesis are very small, the results are distantiated from this bifurcation point and the accuracy may be off.

6

Conclusions and recommendations

6.1. Conclusions

From this thesis several conclusions can be formulated. To structurize these conclusions, the research questions as discussed in section 1.4 are discussed in separate paragraphs. Section 6.2 elaborates on the recommendations. Note that the discussed parameters are based on a model with significant simplifications.

6.1.1. Where do differences regarding global buckling originate between the Eurocode and the DNVGL?

The Eurocode and the DNVGL are different standards, written and defined by different project groups. Therefore, differences are noted within the definition of the buckling checks. However, both checks are based on the same principle:

- Both the Eurocode and the DNVGL define the check as a unity check
- Both the normal force and moments are taken into account;
- The maximum allowed normal force is factorized by a global buckling factor, taking the slenderness and sensitivity to global (Euler) buckling into account;
- Another parameter is introduced to factorize the resistance of a bending moment to account for the slenderness.
- Both checks take several safety factors into account, to allow for small (fabrication) errors.

Comparing both checks using a reference support structure and its turbine as input parameters, the results are as follows:

- Global buckling check DNVGL: $0,0438 \leq 1$;
- Global buckling check Eurocode: $0,022 \leq 1$.

The Eurocode defines that the sensitivity to global buckling is twice as low as the DNVGL. However, both checks also point out that global buckling is very unlikely to occur for designs, compared to the reference wind turbine.
What should be considered is that these checks are executed for one situation only. When a totally different design is subjected to the same checks, other results are expected. However, this does not mean that the global buckling check will ever be an issue for the design of the support structure.

6.1.2. How should the buckling length of an offshore wind turbine be chosen?

The buckling length of a beam is defined as follows:

$$L_{buck}(x) = \sqrt{\frac{\pi^2 EI(x)}{F_{buck}}} \tag{6.1}$$

Since this equation contains a non-constant flexural stiffness $EI(x)$, a varying buckling length over the height of the structure is obtained. However, a single value of the buckling length is required for analysis. Two different cases are distinguished:

- A support structure with varying geometry is subjected to a lateral deformation, resulting in the definition of a single flexural stiffness term for the entire structure. Using this term the buckling length is calculated;
- A structure with a constant geometry is defined, embedded in a Winkler foundation. Several different soil conditions are defined and evaluated.

A buckling length of 228 meter is found for the structure with varying geometry. Compared to the length of 104 meter, which is the actual height of the taken structure, it is a factor 2,2 higher. This is higher than the factor 2 that is found for a cantilever beam.

This seemingly high buckling length can be explained by the fact that the actual geometry, and thus the flexural stiffness of the pile varies over the height. Therefore a segmented buckling shape is obtained, corresponding with a long buckling length.

Several soil conditions and penetration depths are defined to create a couple of loadcases. Three soil stiffness's are defined (loose, medium and dense sand), along with 3 penetration depths (15, 28, 50 meter) result in the following buckling lengths:

Table 6.1: Buckling length: soil conditions

Loadcase	**Soil types**	H $[m]$	L_{buck} $[m]$
1.	Loose sand	28	211,75
2.	Medium sand	28	210,00
3.	Dense sand	28	209,10
4.	Medium	15	239,38
5.	Medium	50	209,75

Note that all buckling lengths are more than twice as long as the normal length of the structure (104 meter). A loose soil stiffness results in a longer buckling length than a more dense variation of the soil. This can be explained by means of the buckling shape of the structure. When a shape is inclined at one side and free at the other side, the buckling shape can be mirrored, and the buckling length is taken as twice the length of the pile. Here, however, we have a non-inclined boundary condition. Therefore the buckling shape of the pile is angled at the seabed and the buckling length is different.

Regarding the penetration depth of the pile, the same effect is noticed as with the soil stiffness variation. A larger penetration depth stiffens the structure, which leads to a shorter buckling length. However, when the penetration depth is lengthened to infinity, a buckling length is obtained that is larger than for a cantilever beam. This is explained by the buckling shape: at the seabed the pile is not vertical, hence the buckling shape, and therefore the buckling length is longer.

6.1.3. Is a second order analysis required to determine whether global buckling is relevant in the design of an offshore wind turbine?

The influence of the second order term on the bending and load characteristics is determined by comparing a model with this second order term to one without this term. Figure 6.1 visualizes the displacement, rotation, moment and shear force as determined by the model.

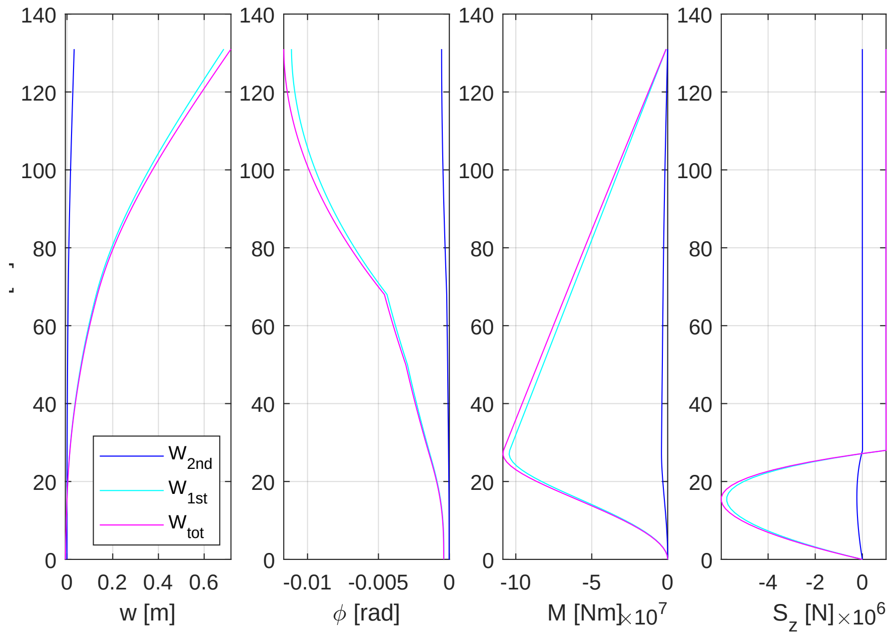

Figure 6.1: Euler buckling final model: Determinant vs m_{top}

Note that the influence of this second order term is very small compared to the first order term. To visualize this effect even further, an incremental load factor is introduced. This factor is calculated as follows, using the moment distributions of resp. the second order term and the first order term. The ILF distribution is given in Figure 6.2.

$$ILF = 1 + \frac{M_{2nd}(x)}{M_{1st}(x)} \tag{6.2}$$

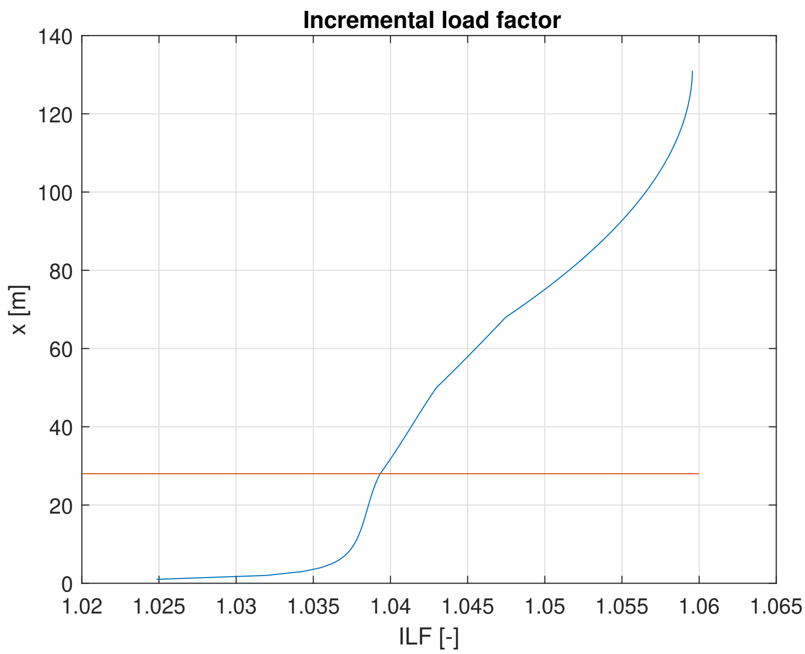

Figure 6.2: Incremental load factor over the height of the pile

The incremental load factor is not higher than 1.06 for the reference turbine, and maximum at the top.

However, to make this ILF usable, one should define a (conservative) value for the ILF, constant over the height of the structure. In this case, one could consider an ILF of 1,05.

Returning to the research question: a second order analysis is in this case not required, since it effects is rather small. However, since there is a trend where larger wind turbines are placed in deeper seas, it might become more relevant (since a higher placed turbine results in a longer support structure, which will bend over more and thus increases the second order term). A manner to take the second order term into account might be the ILF.

6.1.4. When does global buckling become relevant?

This thesis approached this question in three manners:

- Euler buckling
- Global buckling as defined per standards: the global buckling checks;
- Global buckling compared to local buckling.

Figure 6.3 shows the sensitivity to Euler buckling. The cyan vertical line gives the vertical force as result of the top mass. The red vertical lines give the Euler buckling forces. Here it can be noticed that global buckling is unlikely to become a problem. The top mass requires to be increased by a factor 3, without a design change in the support structure, for the pile to fail due to buckling. It is more likely that another fail mechanism will be reached beforehand.

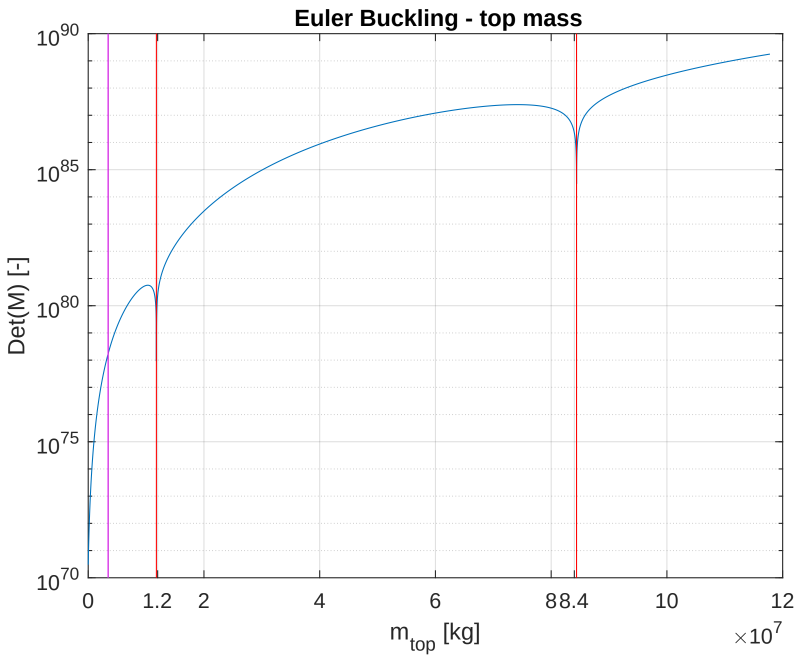

Figure 6.3: Euler buckling forces

Both the global- and the local buckling checks did not approach the relevant zone of the unity checks:

- Global buckling check DNVGL: $0,0438 \leq 1$;
- Global buckling check Eurocode: $0,022 \leq 1$.
- Local buckling check Eurocode: $0,049 \leq 1$.

It can be concluded that in this configuration the checks are not relevant. Other failure modes such as fatigue, are likely to be likely to perform better as guideline to design the support structure.
However, comparing the local- and global buckling check from the Eurocode, it can be seen that the local buckling scores almost twice as high as the global buckling check. Therefore this local buckling check is more relevant in this configuration. If the global buckling check will ever become relevant is doubtful. Other failure mechanisms are more demanding, which are likely to be leading in the design of a support structure.

6.2. Recommendations

From the thesis several recommendations are defined.

Firstly, it s unlikely that the global buckling check will be relevant in the near future in the design of wind turbines. However, this does not mean that it should not be taken into account. The currently defined checks are not too complex to perform. Hence it is recommended to keep performing these checks.

When an early design is made and checked for global buckling by means of the Euler buckling equation, typically a buckling length of twice the length of the structure is chosen. However, since it is found that this buckling length is some higher than 2, it might be beneficial to incorporate this small addition in the buckling length. However, how much length should be added is unclear. A large set of designs should be analyzed to determine a generally applicable factor for the buckling length.

An incremental load factor (ILF) may be a good solution to perform the global buckling check using a first order model. This type of model allows for more insight in the properties of the model, and is better approachable for less specialized designers. However, this ILF is likely to be around 1.05, which is not a significant addition to the total amount of bending, moment or shear force. Since analysis of a design of an offshore wind turbine requires more in depth analysis for among others fatigue and other failure modes, a second order model may be available anyway. Therefore analysis with an ILF may be irrelevant, and buckling analysis should be performed following the currently used methods.

Bibliography

[1] EL Axelrad. *Flexible shells.* Springer, 1980.

[2] Subhamoy Bhattacharya. *Design of Foundations for Offshore Wind Turbines.* Wiley, 2019. ISBN 9781119128151. doi: 10.1002/9781119128137.

[3] DNV.GL. DNVGL-ST-0126 : Support structures for wind turbines. *Dnv Gl As*, (April 2016), 2016.

[4] Eurocode. Eurocode 3: Design of steel structures - Part 1-1: General rules and rules for buildings. *Eurocode 3*, 1(2005):91 pp, 2005. doi: [Authority:TheEuropeanUnionPerRegulation305/2011,Directive98/34/EC,Directive2004/18/EC].

[5] Eurocode. Eurocode 1993-1-6. 1(2005), 2011.

[6] GL. Germanischer Lloyd Guideline for the Certification of Offshore Wind Turbines. *Germanischer Lloyd Industrial Services GmbH*, pages 1–480, 2005. URL `http://onlinepubs.trb.org/onlinepubs/mb/Offshore{%}5CnWind/Guideline.pdf{\protect\T1\textdollar}{%}5C{\protect\T1\textdollar}npapers2://publication/uuid/E0736FDA-F8F7-433A-9802-B8519EE5E0A4`.

[7] P. R. Heyliger and J. N. Reddy. A higher order beam finite element for bending and vibration problems. *Journal of Sound and Vibration*, 126(2):309–326, 1988. ISSN 10958568. doi: 10.1016/0022-460X(88)90244-1.

[8] J. Jonkman, S. Butterfield, W. Musial, and G. Scott. Definition of a 5-MW Reference Wind Turbine for Offshore System Development. (February), 2009. ISSN 01487299. doi: 10.2172/947422. URL `http://www.osti.gov/servlets/purl/947422-nhrlni/`.

[9] J.M.J Journee and W.W Massie. *Offshore Hydromechanics.* Number January. Delft, first edition, 2001. ISBN 9781457717659. doi: 10.1109/ICSENS.2012.6411159.

[10] a a Kerciku, S Bhattacharya, H J Burd, and Z a Lubkowski. Fixity of Pile Foundations in Seismically Liquefied Soils for Buckling Calculations – an Eigenvalue Analysis. *The 14th World Conference on Earthquake Engineering*, 2008.

[11] Rafał F Obrzud and Andrzej Truty. The Hardening Soil model - A practical guidebook. 05:205, 2018.

[12] Offshorewind.biz. DONG Explains the Thinking Behind Subsidy-Free Bids, 2017. URL `https://www.offshorewind.biz`.

[13] T Bart Quimby. *A Beginner ' s Guide to the Steel Construction Manual.* Number August. 2011. ISBN 9780615521329.

[14] R.C.Hibbeler. *Mechanics of Materials.* Seventh edition, 2008.

[15] T. Sarpkaya. Force on a circular cylinder in viscous oscillatory flow at low Keulegan-Carpenter numbers. 165:61–71, 1986.

[16] A. S. Sayyad, Y. M. Ghugal, and P. N. Shinde. Stress analysis of laminated composite and soft core sandwich beams using a simple higher order shear deformation theory. *Journal of the Serbian Society for Computational Mechanics*, 9(1):15–35, 2015. ISSN 18206530. doi: 10.5937/jsscm1501015S.

[17] Marc Seidel, Sven Voormeeren, and Jan-Bart van der Steen. State-of-the-art design processes for offshore wind turbine support structures. *Stahlbau*, 85(9):583–590, 2016. ISSN 00389145. doi: 10.1002/stab.201610404. URL `http://doi.wiley.com/10.1002/stab.201610404`.

[18] Project Upwind. Support Structure Concepts for Deep Water Sites. *Project UpWind*, pages 1–210, 2011.

[19] Hans Welleman. Constructiemechanica 3 Module : Stabiliteit van het evenwicht Deel 1 : Theorie December 2007. (December), 2007.